UNIVERSITY OF CALIFORNIA SAN DIEGO

Studying the Central and Peripheral Nervous Systems in larval and juvenile *Berghia stephanieae*

A Thesis submitted in partial satisfaction of the requirements
for the degree Master of Science

in

Marine Biology

by

Carl Arthur Whitesel IV

Committee in charge:

Professor Deirdre Lyons, Chair
Professor Ryan Hechinger
Professor Greg Rouse

2021

The thesis of Carl Arthur Whitesel IV is approved, and it is acceptable in quality and form for publication on microfilm and electronically.

University of California San Diego

2021

DEDICATION

This thesis is proudly dedicated to:

My parents, who helped nurture my passion and curiosity. I couldn't have done this without your love and encouragement.

My sister, for her endless supply of jokes.

My grandparents, for their genuine interest in my work and loving support.

Dr. Deirdre Lyons and Dr. Hereroa Johnston, for their mentorship and support.

All animals involved this study, whose sacrifices to advance scientific knowledge are recognized and valued immensely.

TABLE OF CONTENTS

LIST OF FIGURES

ACKNOWLEDGEMENTS

I would like to thank Dr. Deirdre Lyons and Dr. Hereroa Johnston for their guidance and support throughout this project and my time as an undergraduate in the Lyons Lab. I would also like to thank the Hamdoun Lab at Scripps Institution of Oceanography for use of their confocal microscope, Phil Zefroski, and the Birch Aquarium for providing *Exaiptasia sp.*.

Chapter 1, in part, is currently being prepared for submission for publication of the material. Whitesel, CA; Johnston, HT; Ramirez, MD; Katz, PS; Lyons, DC. The thesis author was the primary investigator and author of this material. Park Masterson of the Lyons Lab provided panel A of Figure 1.3. Dr. Desmond Ramirez provided panels B, C, and D of Figure 1.3.

Chapter 2, in part, is also currently being prepared for submission for publication of the material. Whitesel, CA; Johnston, HT; Lyons, DC. The thesis author was the primary investigator and author of this material. This thesis was funded through NIH BRAIN U01-NS108637, SDB Emerging Research Organisms Grant (2019), and the Scripps Institution of Oceanography Graduate Department.

ABSTRACT OF THE THESIS

Studying the Central and Peripheral Nervous Systems in larval and juvenile *Berghia stephanieae*

by

Carl Arthur Whitesel IV

Master of Science in Marine Biology

University of California San Diego, 2021

Professor Deirdre Lyons

The use of nudibranchs as experimental species for neuroethology has been pivotal to elucidating the basis of behavior. These shell-less molluscs are particularly well-suited, given their swimming and crawling behaviors and large, identifiable neurons. However, little is known about early life stages: how the neural system controls behavior during embryonic, larval, and juvenile stages

remains unclear, mostly due to the intractability of embryos in species currently used for behavioral studies. Understanding central nervous system development and the formation of identifiable neurons are crucial for neuroethological studies. However, the embryonic origins of the central nervous system and the appearance of identified neurons after metamorphosis are unknown. Therefore, the aeolid nudibranch Berghia stephanieae has been established as an experimental system; this species' embryos are accessible, enabling the study of brain development. This study reports on methodology for labeling the central nervous system with various antibodies that recognize neurotransmitters, creates the most detailed larval and juvenile staging system in a nudibranch to date, and describes the expression patterns of neurotransmitters in the brain during these stages. The post-metamorphic juvenile brain is organized similarly to the adult brains of nudibranch neuroethological models. Gangliogensis of the larval and juvenile central nervous systems is described and quantified. Additionally, the central and peripheral nervous systems are described in detail throughout distinct larval and juvenile stages. Finally, landmark neurons were identified in post-metamorphic stages. These results provide a detailed atlas of neural development and quantification of those growth through ganglion cell counts and immunoreactive cell counts throughout time.

Introduction of the Thesis

Like many other gastropods, nudibranchs are morphologically diverse. One group of nudibranchs, aeolid nudibranchs, are generally identified by their morphology. Aeolid nudibranchs are defined by paired oral tentacles, paired sensory structures that resemble a slim finger, which extend from the anterior end of the face. Additionally, paired rhinophores, club shaped sensory organs, are located at the anterodorsal face, and numerous cerata, extensions of the digestive tract with hypothesized defensive functions, which are clustered along the lateral sides of the body (Kristof & Klussman-Kolb, 2010) (Carrol & Kempf, 1990). In addition to serving a digestive function, the cerata are also highly innervated and sequester nematocysts in a possible defensive role (Miller & Byrne, 2000). Other nudibranchs, such as dorid nudibranchs, do not generally have these cerata or oral tentacles (Valdes, 2002).

Berghia stephanieae is an aeolid nudibranch with stereotyped oral tentacles, cerata, and rhinophores. It is found off the coast of Florida and is commonly bred in aquaria for the removal of the anemone *Exaiptasia diaphana*, which is its natural prey. These nudibranchs are approximately 3 cm in length at the adult stage and lay egg masses densely packed with embryos. These whorls are typically laid onto the surface of the water or onto a substrate. Within each egg mass, individual embryos are locked within a strong capsule that slowly weakens throughout time. Within a single whorl, there is noticeable developmental asynchrony. There is a roughly 4 day window for metamorphosis to occur when an

egg mass is raised at 24°C due to this asynchrony. Eventually, around metamorphosis, the capsule is weakened enough for the embryos to break free.

B. stephanieae follows a typical metamorphic process for nudibranchs (Bonar & Hadfield, 1974). Generally, nudibranchs reach a larval, veliger stage, and after settlement, begin to lose their velum, detach from the shell, and undergo detorsion, the unwinding of the twisted visceral loop and adjusts the location of the anus (Minichev, 1970). Then, the velum-less nudibranch contracts its now elongated body and pulls itself out of the shell. The foot fuses with the visceral mass as the juvenile nudibranch begins to elongate (Bonar & Hadfield, 1974). In B. stephanieae, the velar rudiment precursor to the velum forms at 2.2 days at 24°C and assumes a bilobed shape at 3.3 days. Then, at 7.4 days, the propodium, an anterior projection of the foot, forms. This is the last morphological characteristic of B. stephanieae development before hatching at 11.6 days and metamorphosis at 13 days (Carroll & Kempf, 1990). Unlike similar nudibranchs such as *Phestilla* (Hadfield & Pennington, 1990), *B. stephanieae* does not require an environmental cue to metamorphose by a habitat-specific inducer (Carroll & Kempf, 1990). After metamorphosis, the oral tentacles, rhinophores and cerata rapidly develop as the animal elongates. Additionally, both circular and oblique body muscles begin to develop after metamorphosis as the larval retractor muscles begin to decay. These body muscles allow the juvenile and future adult stages to contract and elongate in a worm-like fashion (Kristof & Klussman-Kolb, 2010). These foundational works allow for neural studies using these

developmental stages, a feature which is not easily achieved in other nudibranch neural models.

Invertebrates, including gastropods, have been used as neural models for their well-studied neural behaviors and stereotyped central nervous system (Newcomb, 2006) (Wastson, 2020). Invertebrate systems have been crucial in key advances in neuroscience such as Schwann cells which sheath axons (Geren & Schmitt, 1954) and axon guidance (Araújo & Tear, 2003) (Whitington, 1993). One of the most promising uses of invertebrate neural models is the ability to understand the neural circuitry of every neuron within the brain to elucidate the roles they play within neural circuits leading to a behavioral output. However, to reach this end goal, it is important to understand when the neuroanatomy of these models form. When gangliogensis occurs, how the peripheral nervous system develops, and how and when neural circuitry forms is crucial to truly understanding the nudibranch brain. This study, in collaboration with the *Berghia* Brain Project, an NIH Brain Initiative (NIH BRAIN U01 NS-108637) seeks to create a detailed atlas of the central nervous system from larval to post-metamorphic juvenile stages of *Berghia stephanieae.*

The larval central nervous system was first identified with nuclear staining at the early veliger stage and all ganglia easily identifiable at the pre-eyed veliger stage. The brain grows in both size and cell count until metamorphosis occurs and the J1A juvenile marks the first stage where the cerebral and pleural ganglia in the larval CNS merge into the cerebropleural ganglia of the post-metamorphic CNS. In

addition to this merge, the apical organ, one of the first ganglia to form during development (Carrol & Kempf, 1996), is lost at metamorphosis while the rhinophore ganglia are formed. Additionally, at post-metamorphic juvenile stages, small cardioactive peptide b-*like* (SCPb) and serotonin-*like* immunoreactive neurons were consistently located between the three juvenile stages analyzed. Some of these located neurons were formed and some lost in between this small time interval. The peripheral nervous system also underwent a significant reorganization after metamorphosis. Before metamorphosis, peripheral nervous system immunoreactivity was limited to the mantle edge tissue, and projections from the apical organ and pedal ganglia. However, after metamorphosis, numerous projections from the cerebropleural and pedal ganglia heavily innervate the foot. Additional projections from the cerebropleural ganglia also innervate the buccal region. Finally, elongated cilia, never before described, were identified on the surfaces of the forming oral tentacles and rhinophores. While their exact function is unknown, they appear to exclusively mark these sensory organs and likely play a function within the PNS.

Chapter 1: Formation of the CNS and identifiable neurons in *Berghia stephanieae*

Abstract

Nudibranchs and their other heterobranch relatives have been widely used as neural models. These neural models are useful due to identifiable neurons within the central nervous system (CNS) and a stereotyped CNS between species. Identified neurons have been used to advance understanding of neurotransmitters and the neural basis of behavior. However, current gastropod neural models are only utilized at adult stages due to difficulties rearing these species in the lab. Here, the larval and juvenile stages of the nudibranch *Berghia stephanieae* are used to answer one of the unsolved questions of nudibranch neurobiology: when are identified neurons, and the ganglia they form, born during development? In addition, a developmental staging system of 9 larval and juvenile stages was established to create a detailed atlas of immunoreactivity throughout development. Gangliogensis occurs at or before the early veliger stage, when the first CNS ganglia were identified. The early veliger stage has a total of 130 ± 12 cells (standard deviation) while the J1C juvenile has 752 ± 63 cells in the CNS. After metamorphosis, 6 distinct neuronal identities were described in the cerebropleural ganglia throughout the 3 studied juvenile stages. Small cardioactive peptide b-*like* (SCPb) and serotonin-*like* immunoreactive patterns were analyzed for 9 developmental stages from before gangliogensis, through the formation of the adult CNS ganglia in the J1C juvenile. These tools will allow for comparisons across developmental time and between different gastropod species to further

elucidate the origin of identified neurons, neural circuits associated with them, and the resulting behavioral outputs.

Introduction

Gastropod neurons in the central nervous system generally exhibit neurons with their soma on the outside of the ganglion and projections of their axons internally. Some of these neurons can be reliably identified by their large soma, distinct neuropeptide immunoreactivities, homologous locations between different species, or a combination of the three (Katz & Quilan, 2019). These traits have enabled a deep understanding of neural circuitry that leads to behavior formation, especially the swim pattern generator circuit. In many gastropods, the neurotransmitter serotonin is a consistent marker of sets of identified neurons and has been shown to have a direct role in locomotion in adult nudibranchs (Newcomb, 2006 & 2007). Small cardioactive peptide b (SCPb), a molluscan specific neuropeptide, is also commonly used as a marker of identified neurons (Watson & Willows, 1992) (Llyod, 1987) and has also been shown to modulate locomotion in addition to the esophagus (Watson, 2020). Additionally, these identifiable neurons have allowed for comparisons between species of nudibranch with homologous identifiable neurons.

However, identifying and studying neurons in gastropod models has been largely limited to adult animals (Bulloch & Ridgway, 1995). Without a timeline of gangliogensis and comparable immunoreactivity patterns throughout development, identified neurons, neural circuitry, and behavioral studies have not been expanded from the adult to earlier developmental stages in nudibranchs. By

expanding the study of molluscan brains earlier in development, the birth of identifiable neurons, neural circuitry, and the behaviors they create can be studied throughout development and compared between nudibranch species. Here we create a detailed neural atlas of serotonin-*like* and SCPb-*like* immunoreactivity (-*lir*) in the central nervous system from pre-gangliogensis to the formation of the juvenile CNS ganglia after metamorphosis. All nudibranchs currently used as adult neural models have either never been reared from eggs in the lab or are too large to efficiently grow large populations in the lab. Thus, we use the nudibranch *Berghia stephanieae*.

Berghia stephanieae is an aeolid nudibranch commonly used in the aquarium hobby industry to remove the anemone *Exaiptasia diaphana* (Monterio, et. al, 2020). *B. stephanieae* is easily culturable due to its small size, rapid egg mass production, and easily collected prey anemone. Embryos are easily distinguished through easily identifiable morphological features which allow for easy developmental stage selection (Carroll & Kempf, 1990). In addition, adult *B. stephanieae* have the distinctly large neuron cell bodies, unique neuropeptide identities, and identifiable neurons seen in other gastropod neural models (Figure 1.3, C). Previously a coarse description of the rearrangement of the larval CNS after metamorphosis had been documented in *Berghia* (Carroll & Kempf, 1996). To sufficiently describe the development of the central nervous system, identify the birth of identified neurons, and describe when ganglia formed in the CNS, an exhaustive staging system needed to be created.

In order to account for asymmetrical development within a single egg mass, animals were staged by distinct, plate-level morphological features. These features were first identified using differential interference contrast (DIC) microscopy and scanning electron microscopy (SEM). Then, the stages developed by key morphological characteristics were investigated with DAPI and other morphological stains to identify CNS ganglia and confirm distinct morphological features that defined each stage. Finally, with these stages fully analyzed, neural antibodies were used to describe immunoreactivity patterns in the CNS at these stages. Using this approach, four important questions were answered:

- How do ganglia grow throughout development and during metamorphosis?
- When do identified neurons arise during development?
- Does the peripheral nervous system (PNS) arise before the CNS?
- What is the actual neuroanatomy of Berghia and when does the visceral ganglion merge with the cerebropleural ganglion?

How do ganglia grow throughout development and during metamorphosis?

While previous studies have identified the changes to the nervous system in *B. stephanieae* before and after metamorphosis (Carroll & Kempf, 1990), limited temporal resolutions in those previous studies prevented analysis of initial CNS gangliogenesis and identification of when the adult CNS ganglia form during metamorphosis. The ganglia of the post-metamorphic CNS resemble that of the adult (Carrol & Kempf, 1990) allowing for behavioral, immunoreactivity, and neuroethology studies comparisons between these developmental stages. Despite morphological differences of the body plan overall, the larval stage contains most of the ganglia that will eventually form the post-metamorphic CNS. Understanding how and when these ganglia form is important for further studies regarding the genesis of neural circuitry and behaviors. Additionally, the growth of these ganglia has never been measured. Through every stage of development, the CNS ganglia are all sized differently. Quantifying the growth of these ganglia throughout development can provide additional insight into the importance and emergence of key behaviors. Additionally, studying the growth of the central nervous system throughout its rapid transformation during metamorphosis is crucial to understand how the adult CNS emerges from the larval CNS.

When do identified neurons arise during development?

Identified neurons have been a key component of gastropod neural studies for decades and have contributed greatly towards the understanding of gastropod neuroethology (Watson, et. Al, 2020), (Watson, 2002). Identified neurons provide a level of homology that cannot be easily accessed in species without identified neurons. They allow for direct comparisons of neural circuitry between species with different behaviors, CNS circuitry, and body plans (Newcomb & Katz, 2001) (Sakurai, et. al, 2011), (Newcomb et. Al, 2006). However, current gastropod neural model species containing identified neurons are not suitable for developmental studies due to difficulty rearing animals to adulthood in the lab. Other studies (Dickinson et. Al, 1999) (Voronezhskaya & Elekes, 2003) utilizing rearable gastropods such as the pond snail *Lymnaea stagnalis* and slipper snail *Crepidula fornicata* have clusters of immunoreactive neurons at larval and post-metamorphic stages but no identifiable neurons were located at larval or juvenile stages. However, neurons were consistently located in juvenile stages of *Berghia stephanieae*. Individual neurons, located in distinct positions, were found consistently between replicates and were traceable through post-metamorphic stages. Describing these neurons and their neural circuitry will allow for future studies to trace these neurons through development to the adult stage and to compare the circuitry of these neurons between the juvenile and adult stages.

Does the PNS arise before the CNS?

The gastropod peripheral nervous system (PNS) has been described to form earlier than or simultaneously with, the first ganglion to form, the apical organ (Croll & Voronezhskaya, 1996). These neurons are generally accepted as sensory neurons that differentiate at the periphery (Voronezhskaya & Ivashkin, 2010). One hypothesis suggests that these cells provide “scaffolding” for the CNS by guiding neurogenesis along their fibers (Nezlin & Voronezhskaya, 2017). However, neural immunoreactivity has never been studied before the apical organ’s formation in *Berghia stephanieae*. Previous studies have identified FMRFamide (Kristof & Klussman-Kolb, 2010) and serotonin (Kempf, et. Al, 1996) immunoreactivity in the apical organ of *B. stephanieae*, but expression of these two neurotransmitters was limited to the apical organ and no peripheral neurons were identified before formation of the remaining larval CNS. Here we describe two laterally paired SCPb-*lir* neurons that form before the apical organ and run from the dorsal face down towards the future foot. These neurons are hypothesized to serve the same scaffolding function as described previously in other gastropod species.

What is the actual neuroanatomy of Berghia and when does the visceral ganglion merge with the cerebropleural ganglion?

Despite multiple studies (Ellis, 2010) (Carroll & Kempf, 1996) (Klussman-Kolb, 2010) confirming which ganglia are within the CNS ganglia in pre- and post-metamorphic stages of *B. stephanieae*, there are fundamental disagreements regarding when the visceral ganglion merges with the left CPL after metamorphosis. Kristof & Klussman-Kolb, 2010 described the merge of the VG into the left CPL occurring when the post-metamorphic juvenile had slightly elongated more than previous compact larval stages. However, at the same stage Caroll & Kempf, 1994 described a distinct VG located at the posterior end of the left CPL. Additionally, these studies described conflicting descriptions of the buccal ganglia's location, suggesting it was placed as the most anterior ganglion in the larval CNS (Kristof & Klussman-Kolb, 2010) or located much more posteriorly, behind the CPL along the anterior-posterior axis (Caroll & Kempf, 1994). Here, a detailed developmental time series extending from gangliogensis to post-metamorphosis was used to address these disagreements and establish a timeline of neurogenesis within *Berghia stephanieae*. It was determined that the VG is present after metamorphosis and directly behind the left CPL. However, at the J1C juvenile stage, the VG had merged with the left CPL ganglion. Additionally, this study confirmed the placement of the buccal ganglia as described by Caroll & Kempf, 1994. Interestingly, despite the merge of the VG into the left CPL ganglion at the J1C stage, there was no statistically significant difference in the number of

cells when the left and right CPL ganglia were compared, despite the addition of the approximately 34 VG cells.

Methods

Embryo Husbandry and Handling

Adult *Berghia* were grown in bowls approximately 16 cm in diameter. The animals were kept in artificial sea water and grown at 21ºC. Adults were maintained in groups of 5 to 6 and fed a medium sized *Exaiptasia* three times a week. After feeding, the bowl was manually cleaned with a fine paintbrush and the water was replaced. The dishes were covered with a petri dish lid to prevent evaporation.

Adult *Berghia* laid their egg masses at 21ºC and each egg mass was kept intact and raised in bulk. For each experiment, immediately after collection, the encapsulated embryos were freed from the outer sheath of the egg masses and the contents of one egg mass transferred into a well within a 6-well plate in artificial sea water (ASW) at 27ºC to speed up development. Animals were raised from single cell stages to post-metamorphic juveniles. The egg masses were raised separately to better care for each egg mass independently. Embryos were staged by identifying key morphological characteristics, such as the length of the foot, position of the foot relative to the body, visceral mass shape, and crawling behaviors using a Zeiss Stemi 305. This staging system was used to select embryos that met staging criteria to avoid issues caused by developmental asynchrony within the whorl. These characteristics are described in Figure 1.4.

Before fixation, animals from the pre-eyed veliger stage needed to be relaxed. Animals were transferred with 1.5 mL of ASW into one well of a 24 well plate. Then, 0.5 mL of 7.5% MgCl2 in ASW was gently added, drop by drop, for 30 minutes. Then, animals were fixed inside their capsules with 4% PFA added gently, drop by drop, for 2 hours at RT or 24 hours at 4°C. This was followed by 4 washes of 1X PBS for 5 minutes while shaking.

Capsules were removed from fixed embryos prior to immunohistochemistry. The capsule removal procedure was stage-dependent; for stages prior eyed-veliger, a 60mm petri-dish were used. The bottom was scored with the corner of a glass slide and the resulting ridges were treated for 1 minute with a solution of 1% protamine sulfate (Millipore Sigma, P4020) and then rinsed with DiH_2O prior to adding embryos. 1X PBS was added and embryos were gently aligned along the score line and allowed to attach for 1 minute. Capsules were peeled off the embryo using a #00 insect pin (Leaflying) by gently piercing through the capsules while avoiding damaging the embryo (Figure 1.2). For the pre-eyed veliger and later stages, a pasteur pipette was pulled to a diameter slightly smaller than the capsule size. The embryos were gently sucked in and out of the pipette, one by one, until the capsule was removed (Figure 1.2). After capsule removal, embryos did not stick to dishes or pipettes, but some stickiness was noted in TDE solutions. To prevent any embryos sticking to dishes or pipettes, all dishes and pipettes were filled with gelatin, drained and left to set overnight. Then, the dishes and pipettes were flushed with DI water several times.

Immunohistochemistry

Before antibody staining, embryos were permeabilized with 1% Triton-X100 diluted in 1X PBS for 1 hour and washed 4 times with 1X PBS for 5 minutes while shaking. Samples were then transferred from 1X PBS to a blocking solution (4% Normal Goat Serum, 5% Bovine Serum Albumin, and 0.1% Tween 20 by volume diluted in 1X PBS) for 1 hour RT or overnight at 4°C. The serotonin-*like* primary antibody was diluted to 1:200 and the SCPb-*like* antibody was diluted to 1:50 in blocking solution. Embryos were incubated for 48 hours at 4°C and the primary antibodies washed 4 times in 1X PBS. Secondary Antibodies conjugated with different Alexa Fluor dyes (488 Donkey anti-Rabbit, 594 Donkey anti-Mouse, or 647 Donkey anti-Rat) (Thermofisher Scientific) were diluted 1:500 in blocking solution containing a working concentration of 0.15 µM DAPI and 100 units/assay of Phalloidin, after evaporation of methanol Phalloidin was prepared in.

Imaging

Samples were cleared by transferring between a series of 35mm petri-dishes of 30%, 60%, and 97% TDE (2,2′-thiodiethanol,166782) (Aoyagi, et. al, 2015) diluted in PBS for 15 minutes each. Animals were moved between the TDE dilutions with a pulled pasteur pipette coated with glycerol. Because of density differences, the animals remained suspended in the small volume of lower percent TDE they were transferred in. To prevent this, the embryos were moved to a different part of the dish with the pulled pasteur pipette. For early veliger and younger stages an additional 12h in 97% TDE was required at 4°C. TDE clearing should be performed after DAPI staining and several washes of 1X PBS. Additionally, TDE causes slight deterioration of DAPI staining quality over time. Anecdotally, TDE incubations of up to 12 hours were tested and the DAPI staining were still viable, but slightly fuzzy.

Embryos were mounted directly in 97% TDE between two coverslips, a 25mm x 50mm coverslip was used as base and a 18mm x 18mm coverslip on top with clay feet. These coverslips were then placed into a custom 3d printed slide holder. This setup allowed both sides of the samples to be easily imaged by flipping the mounting device (Alessandri, 2017). More details can be found in Figure 1.1. Differential interference contrast (DIC) images were collected on a Zeiss Axio Imager M2 using a 20x air objective and fluorescence images were collected using a Zeiss LSM 700 with 20x air objective or a 40x water immersion objective.

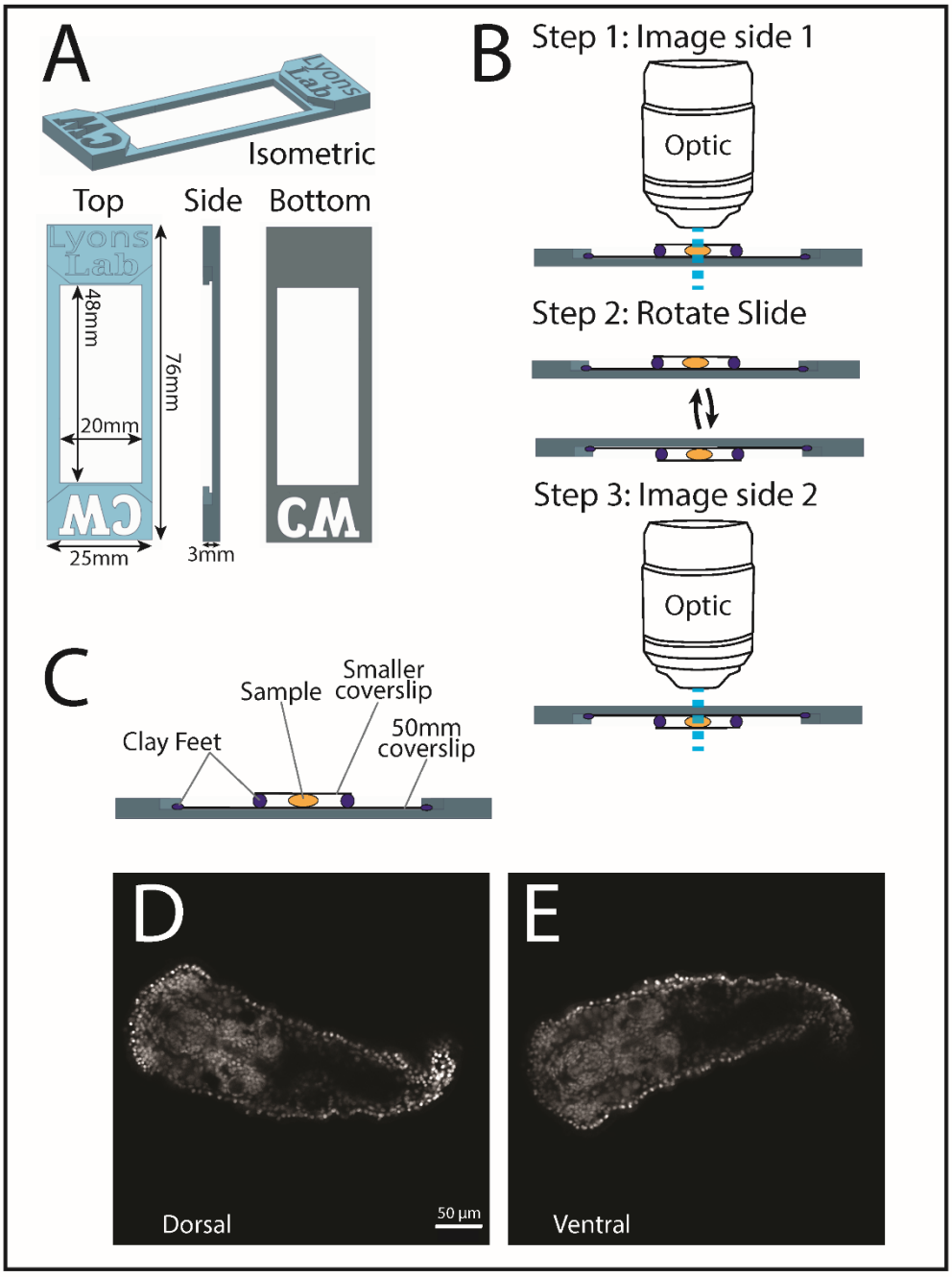

Figure 1.1 A custom 3D printed imaging system

(A) Views and dimensions of 3D printed slide holder. (B) Imaging steps. (C) Cartoon depicting mounted sample in slide holder. (D) Confocal microscopy of DAPI as an example of flipped imaging capabilities.

Image processing and analysis

Differential interference contrast images were focus stacked using Helicon Focus (HeliconSoft) using the pyramid rendering method with a smoothing value of 3. For fluorescent images, cells were manually counted from nuclear staining using ImageJ and the cell counter plugin. (Figure 1.2) Neural immunoreactive cells were identified by presence of a nucleus surrounded by neural immunoreactivity. For neural cell localizations, these immunoreactive cells were positionally mapped with a dot onto a mask in Adobe Photoshop that was drawn to represent the stereotyped CPL ganglion at each stage. that was drawn to represent the stereotyped CPL ganglion at each stage.

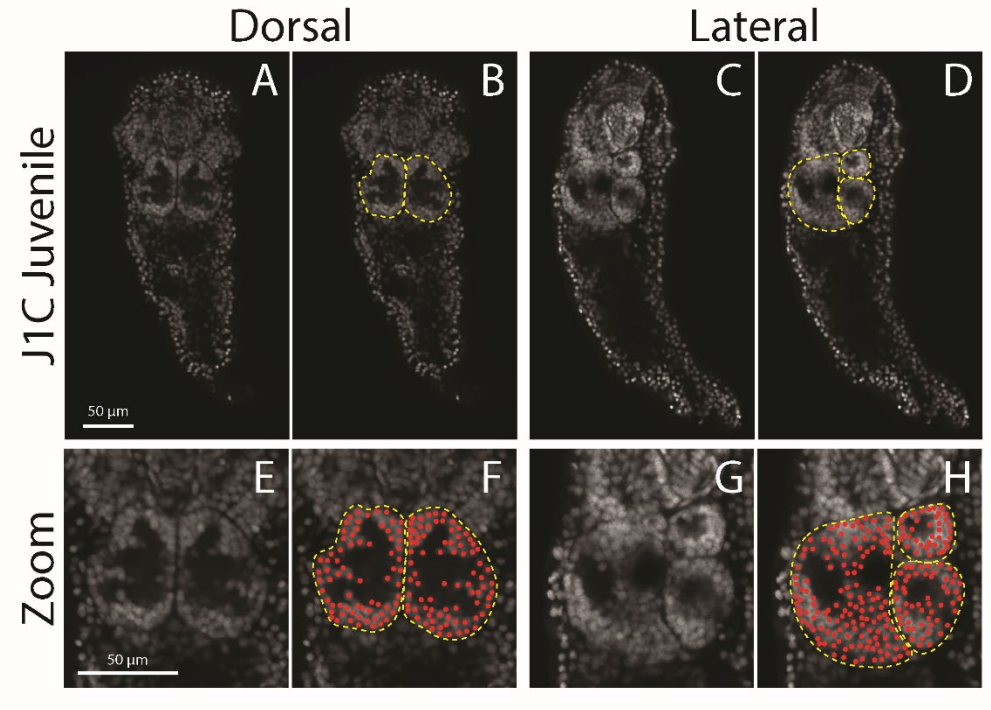

Figure 1.2 Marking and counting cells within the CNS

(A, B, E, F) Dorsal views of DAPI stained J1C Juvenile. (C, D, G, H) Lateral views of DAPI stained J1C Juvenile. Yellow outlines mark the CNS ganglia. Red dots mark individual cells in the CNS ganglia.

Defining ganglia during development

Previous studies in *Berghia* had documented the CNS ganglia's locations at unspecified larval and juvenile stages (Carroll & Kempf, 1996) (Kristof & Klussman-Kolb, 2010). In order to locate these ganglia at defined developmental stages, we used DAPI counterstaining and a set of criteria were developed for identifying a ganglion. First, a ganglion consisted of a clustered group of nuclei that formed a distinguishable shape. Second was a lack of nuclei in the center of the shape, where the neuropil filled the ganglion as seen by densely packed immunoreactive axons Third, with the exception of the visceral and apical organ, the CNS ganglia were laterally paired. Fourth, previous publications were used as a basis for identification of the ganglia at morphologically similar stages and then traced backwards through earlier developmental stages. Ganglia were outlined by choosing the most representative confocal stacks and outlining the ganglion within Adobe Illustrator. (Figure 1.2)

Detailed methodology for relaxation, fixation, immunohistochemistry, and mounting.

Relaxation

To prevent any embryos sticking to dishes or pipettes, all dishes and pipettes were filled with gelatin, drained and left to set overnight. Then, the dishes and pipettes were flushed with DI water several times. Relaxation is somewhat difficult with older veligers and juveniles (Propodium veliger and later). specimens from the pre-eyed veliger stage and later require relaxation. All pasteur pipettes and plates were coated with gelatin prior to use. First, drain 50% of the existing sea water volume from one well of a 24 well dish, leaving approximately. Then, add around 500 µL 7.5% $MgCl_2$ (in FSW) to the embryos into one well of a 24 well plate. Place the glass pasteur pipette against the wall of the well and gently squeeze the bulb to produce a steady stream of liquid that does not make the liquid turbulent. The final result should be a 1:1 of 7.5% $MgCl_2$ and filtered sea water. Wait for 30 minutes to 1 hour then proceed to fixation.

For more sensitive stages, such as older veligers and juveniles, they will appear slightly contracted even with a very delicate addition of $MgCl_2$. This is normal and they will slowly stretch out over the next hour. If J1C juveniles appear heavily contracted, or were mid-turn when $MgCl_2$ was added, place a bright light next to the well. The specimens will slowly straighten out as they travel towards the light. Remove the source after 10-15 minutes to prevent the specimens contracting after reaching the source. J1A and J1B juveniles do not contract as

noticeably. J1A juveniles especially can be treated rougher than any other of the late development stages analyzed here. J1B contraction will only appear on the foot. Towards the center of the ventral surface a small half circle will form as the foot contracts. The remainder of the body will not contract.

Fixation

After relaxing, the liquid in the well was drained to a minimal amount, while still leaving enough liquid to keep the embryos fully submerged. Then, approximately 1 mL of the chosen fixative was added to the well using a pulled pasteur pipette to add slowly, as done in the relaxation steps. The plate lid was placed back on. PFA was added faster than the $MgCl_2$, but still slowly. Care needs to be taken to either relax the specimens fully to allow for slow PFA addition. The specimens were left in PFA for 10-15 minutes, then shaken on an orbital shaker for 2 hours at RT, or incubated without shaking for 24 hours at 4 C. specimens were shaken at a speed where the liquid rotates but does not touch the lid, approximately one third of the maximum speed. Two orbital shakers were used. One was 3D printed using these instructions: https://www.thingiverse.com/thing:3142779 After fixation, specimens were washed 4 times with 1X PBS while shaking at RT. A pulled pasteur pipette was used to remove most of the volume, leaving enough liquid to keep the embryos fully submerged. Then, 1X PBS was added for 10-15 minutes while shaking at RT.

PFA fix was created by diluting 16% PFA glass vials into ASW to a final 4% concentration. 16% PFA was only used within 1 month of opening the glass vial. 4% PFA fixative was made fresh weekly.

PLP (Periodate-Lysine-Paraformaldehyde) fixative uses a 4% PFA base with added chemicals. It was originally created for ultrastructure experiments. PLP was used for SCPb and 5HT antibodies, which were found to react better using

this fixative. It was compatible with all other morphology antibodies used. 7.5 mL of 1X PBS was added to a 15 mL conical tube. Then, 0.185 grams of Lysine HCl (TCI Chemicals, L0071) was added along with 0.022 grams sodium periodate (Thermo Fisher, 20504). 2.5 mL of 16% PFA was added for a final concentration of 4% PFA. The tube was shaken until mixed fully. Then, the pH was adjusted to 7.2-7.4 using sodium hydroxide. This fixative can only be stored for one week.

EDAC fix has no PFA in it. Used for Histamine and GABA Immunostar antibodies. 12.5 mL of PBS is poured into a 15 mL conical tube. Then, 0.25 grams carbodiimide (EDAC) (Thermo Fisher, E2247) and 0.05 grams n-hydroxysuccinimide (NHS) (Thermo Fisher, 24500) are added and mixed. This fixative should be made fresh for each usage. After fixation, embryos were stored in PBS at 4 C. Embryos were never used for immunohistochemical experiments if left for over 3 weeks.

Capsule Removal

After relaxation and fixation, early stages (trochophore to the early veliger stage) were decapsulated using a #00 insect pin. A plastic petri dish of any size was scored using the corner of a glass slide to make a scratch deep enough to hold the embryo. The scratch was treated with 1% protamine sulfate in DiH_2O (Millipore Sigma, P4020) for 1 minute and then rinsed with DiH_2O prior to adding embryos. 1X PBS was added to flood the dish and embryos were gently aligned along the score line and allowed to attach for 1 minute. The capsules were gently pierced and flicked off the specimens. Care was taken to not damage the embryo. Best results were achieved with a #00 insect pin that was bent into a shepherd's hook shape. The capsule was punctured with a gentle pulling motion and then peeled off the embryo. When significantly damaged, capsules were also able to be removed using the pasteur pipette method described below.

After relaxation and fixation, later stages (pre-eyed veliger to propodium veliger stages) were decapsulated with a pulled pasteur pipette. A pasteur pipette was pulled to a final diameter just slightly larger than the capsule itself. Some embryos were slightly larger than the needle. Make sure that the shell enters parallel to the needle. The best pipettes can be identified when on compression of the rubber bulb, the capsule is ejected before the embryo. This represents a clean removal of the capsule and a perfectly sized pipette.

To prevent embryos sticking to dishes or pipettes, all plastic dishes and pasteur pipettes were filled with 1X gelatin, drained and left to set overnight. Then,

the dishes and pipettes were flushed with DI water several times. The fixed embryos were placed into a petri dish with 1X PBS with an unpulled pasteur pipette. Then, using a rubber bulb on the back end of the pipette, the embryos were sucked in and out. The capsules were physically sheared off the embryos without any noticeable damage.

Immunohistochemistry

Before antibody staining, embryos were permeabilized with 1% Triton-X100 diluted in 1X PBS for 1 hour while shaking. Then, the specimens were washed 4 times with 1X PBS for 5 minutes while shaking. Specimens were then transferred from 1X PBS to a blocking solution (4% Normal Goat Serum, 5% Bovine Serum Albumin, and 0.1% Tween 20 by volume diluted in 1X PBS) for 1 hour RT or overnight at 4°C in a 24 well plate.

The serotonin-like primary antibody was diluted to 1:200 final dilution and the SCPb-like antibody was diluted to 1:50 final dilution in blocking solution. (SCPb stocks are diluted 1:1 in glycerol and serotonin stocks are diluted 1:10 in DiH2O). Embryos were incubated for 48 hours at 4°C using the 24 well lid to prevent evaporation. While some condensation did form on the lids, there was not significant condensation. The 24 well plates used had small spaces between the wells that allowed for any spillover liquid to pool. Then, embryos were washed 4 times in 1X PBS for 10-15 minutes while shaking at RT.

Secondary Antibodies conjugated with different Alexa Fluor dyes (488 Donkey anti-Rabbit, 594 Donkey anti-Mouse, or 647 Donkey anti-Rat) (Thermofisher Scientific) were diluted 1:500 in blocking solution. If DAPI or phalloidin was used, it was diluted to a final concentration of 0.15 µM DAPI and 100 units/assay of Phalloidin. Phalloidin stock reconstituted in MeOH was placed into an empty well of a 24 well plate for around 30 minutes in a fume hood to allow the MeOH to evaporate. The plate was covered with aluminum foil to prevent

degradation of the fluorophores. Then the blocking solution with secondary antibodies and DAPI was added and thoroughly mixed. Specimens were washed 2X with 1X PBS for 10-15 minutes while shaking. The 24 well plate was wrapped with aluminum foil to prevent fluorophore degradation. Specimens were normally cleared immediately after secondary antibody treatment, but some specimens were stored overnight in 1X PBS before clearing.

Clearing

TDE clearing (2,2′-Thiodiethanol, Millipore Sigma, 166782) was performed after the addition of secondary antibodies and dyes. TDE causes the slow leech of DAPI staining into the cytoplasm. It is incompatible with Hoechst, which will leak into the cytoplasm immediately after TDE addition. TDE slightly decreased the DAPI nuclear staining quality, but was still viable even after a 12-hour soak. TDE is effective at clearing non-yolky tissues, but struggles to remove yolky tissues, such as the visceral mass of the trochophore through early veliger stages. Then, using a gelatin coated pasteur pipette, the specimens were moved from the 24 well plate to a 60 mm petri dish containing 30% TDE diluted in PBS for 10-20 minutes at RT. After the addition of specimens, the lids are placed onto the petri dishes. Care was taken to not transfer large quantities of liquid with the specimens.

Then, the specimens were moved to a second petri dish containing 60% TDE diluted in PBS for 10-20 minutes at RT. Each transfer used a designated pasteur pipette to prevent any contamination. specimens were individually located using dim lighting. To easily recover the samples, place the specimens into a small group after step 2a to easily relocate them. If the specimen cannot be seen adjust lighting style and brightness and check the rim of the petri dish. When added, the specimens will float in the small amount of lower % TDE added along with the specimens. Gently suck the specimen into a gelatin coated pulled pasteur pipette and replace the specimen away from this area of lower % TDE. When successful,

the specimen will sink and stay. Finally, specimens were moved to a petri dish containing 97% TDE diluted in PBS for 10-20 minutes at RT. In order to effectively image specimens, move specimens through the TDE series in small batches, depending on the speed of imaging. A good rule of thumb is to begin prepping the next batch of specimens when approximately 40 minutes remains on the current imaging batch. Avoid specimens sitting in TDE washes for long periods of time. Mount the specimens onto slides or store in PBS until they are ready to be imaged. Earlier stages, due to how yolky and dense the specimens are, required an additional soak of 97% TDE of up to 12 hours at 4 C.

Mounting specimens

For normal glass slide mounting, animals were mounted with a glass slide and a coverslip. After TDE clearing, specimens were placed onto a glass slide centered in a pea size drop of 97% TDE. TDE is incredibly sticky and care should be taken to clean any working surfaces. Then, a coverslip with clay corners was placed onto the slide. The corners were gently compressed until the specimen gently touched the coverslip. Slowly compress the sample to avoid squishing it. Test compression levels by gently rolling the specimen. Never tap the middle of the coverslip or directly above the sample. To rotate specimens, forceps were used to gently push the coverslip and rotate the specimen along with it.

For custom 3D printed slide holder mounting, animals were mounted with two coverslips. The custom 3D printed slide holder I designed allows for rapid imaging of 2 faces and preserves orientation between both images. This proved useful as delicate specimens did not usually survive 4 attempts at reorientation. After TDE clearing, specimens were placed onto a 50 mm x 25 mm coverslip centered in a pea size drop of 97% TDE. TDE is incredibly sticky and care should be taken to clean any working surfaces. Then, a 18 mm x 18 mm coverslip with clay corners was placed onto the 50 mm coverslip. The corners were gently compressed until the specimen gently touched the 18 mm coverslip. Slowly compress the sample to avoid squishing it. Test compression levels by gently rolling the specimen. Never tap the middle of the coverslip or directly above the sample. To rotate specimens, forceps were used to gently push the coverslip and

rotate the specimen along with it. After orientation the specimen, the arrangement can be slid into the 3D printed slide holder. If the holder is loose, clay can be used to fill the gaps around the 50 mm coverslip. The first side was imaged, flipped, and the second side was imaged. If the specimen is located near the edge of the slide, simply move the 50 mm coverslip to recenter the specimen inside the 3D slide holder's hole. Then, the coverslip arrangement was removed from the 3D slide holder to reorientate the specimen to image the other 2 faces. The reorientation is easiest without the 3D printed slide holder. Use a Kim wipe on one corner of the coverslip to prevent the coverslip from sticking to a glass surface.

Results

SCPb-*lir* and serotonin-*lir* mark identifiable neurons in the adult central nervous system of *Berghia stephanieae*

Using a dissecting microscope, it was determined that the adult *B. stephanieae* has the typical anatomy of an aeolid nudibranch. At the anterior face of the animal, two oral tentacles extend outwards (Figure 1.3, A). These oral tentacles are often swept around as the animal crawls forwards. Dorsally, two paired rhinophores are seen slightly anterior to the eyes (Figure 1.3, A). The rhinophores serve a chemosensory function in nudibranchs (Wyeth & Willows, 2006) (Levy, 1997) (Wertz, 2006) and connect directly to the central nervous system through the rhinophore ganglia.

Berghia, like other gastropods (Newcomb, 2006 & 2007), has four large, bilaterally paired ganglia in the central nervous system of the adult nudibranch (Figure 1.3, B). The rhinophore ganglia, which innervate the rhinophores, are the most dorsal ganglia. Directly posterior and ventral to the rhinophore ganglia are the cerebropleural ganglia. Beneath the cerebropleural ganglia are the pedal and buccal ganglia pairs. Some gastropods possess big identifiable neurons within the CNS ganglia (Katz & Quinlan, 2019). For instance, the cerebropleural ganglia contain neurons that are believed to be polyploid neurons (Shuichi, 2017) and thus are larger than other nuclei in the ganglion (Figure 1.3, C). These large neurons are used as landmarks within the CNS to assist with both interindividual and interspecies comparisons. It is the combination of soma size, soma location, and

neurotransmitter immunoreactivity that can be used to identify distinct neuronal identities between gastropod neural models. Within the cerebropleural ganglia of *Berghia*, a set of identifiable neurons are stained by either serotonin-*like* and SCPb-*like* immunoreactivity (Figure 1.3, D).

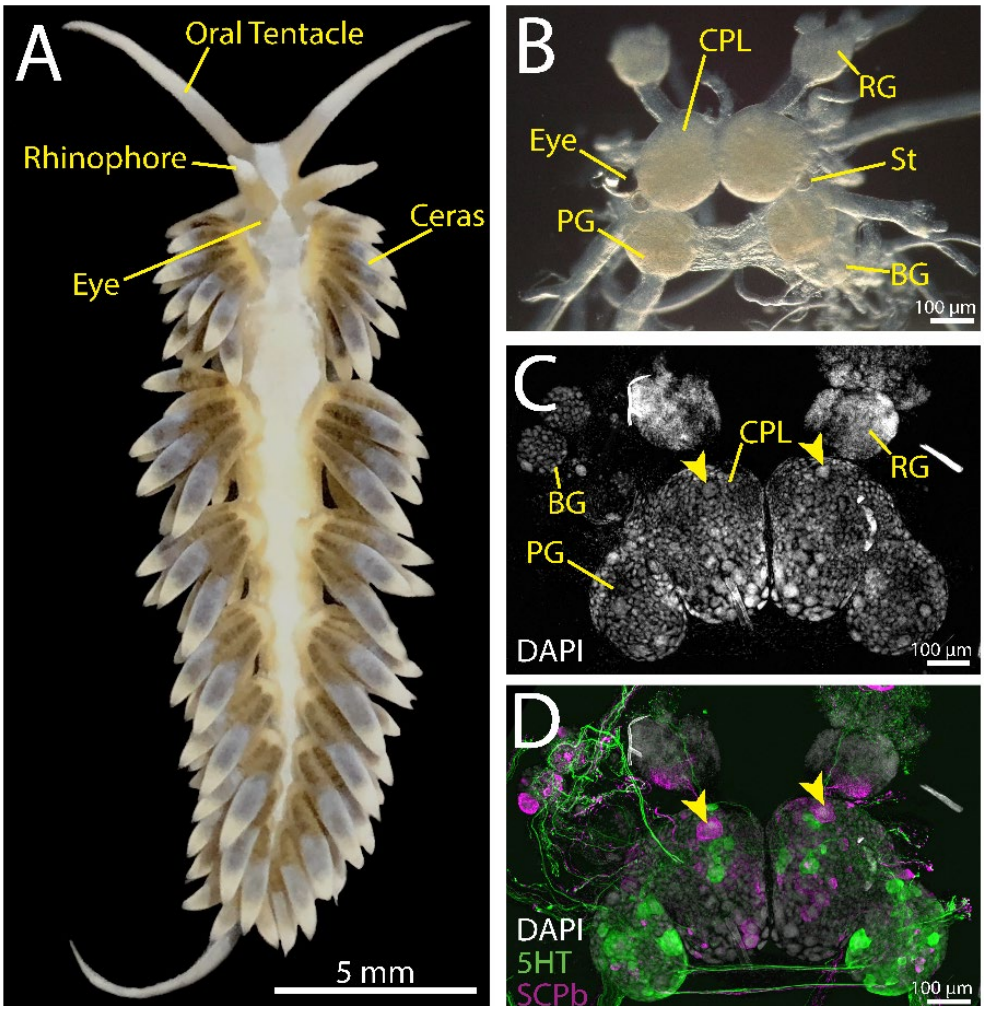

Figure 1.3 SCPb-*lir* and Serotonin-*lir* mark identifiable neurons in the adult central nervous system of *Berghia stephanieae*

Dorsal view of the adult *B. stephanieae* and dissected brain using transmitted light and confocal microscopy. BG, Buccal Ganglion; CPL, Cerebropleural Ganglion; PG, Pedal Ganglion; RG, Rhinophore Ganglion

Morphological changes during development from larval to juvenile stages of *B. stephanieae*

For this study, 9 stages of larval and juvenile development were identified, between 3 and 10 days post oviposition (dpo) when raised at 27°C. The first stage is the trochophore-like stage (Figure 1.4, A), which is reached 0.5 days after gastrulation at 27°C. At 3.5 dpo, the rudimentary veliger stage marks the first appearance of the velum and the formation of the shell gland. The early veliger stage occurs at 4 dpo. First, the velum have separated further from the body and marks the first appearance of the foot. Finally, the visceral mass is now surrounded by the growing shell. At 5 dpo, pre-eyed veligers have developed their velum are distinctly separated from the body and visibly ciliated. The foot also has elongated further. Additionally, the visceral mass is visibly separated into 3 distinct lobes.

Figure 1.4 Morphological changes during development from larval to juvenile stages of *B. stephanieae*

DIC images of fixed samples from the trochophore-like stage to the J1C juvenile stage. All images are scaled according to the 50 μm scale bar (A), inserts are scaled to 25 μm (D insert). BG, Buccal Ganglion; BM, Buccal Mass; CPL, Cerebropleural Ganglion; Ci, Cilia; E, Eye; Ft, Foot; G, Gut; Op, Operculum; OG, Optical Ganglion; PG, Pedal Ganglion; RG, Rhinophore Ganglion; St, Statocyst; V, Velum; VM, Visceral Mass; *, Mouth

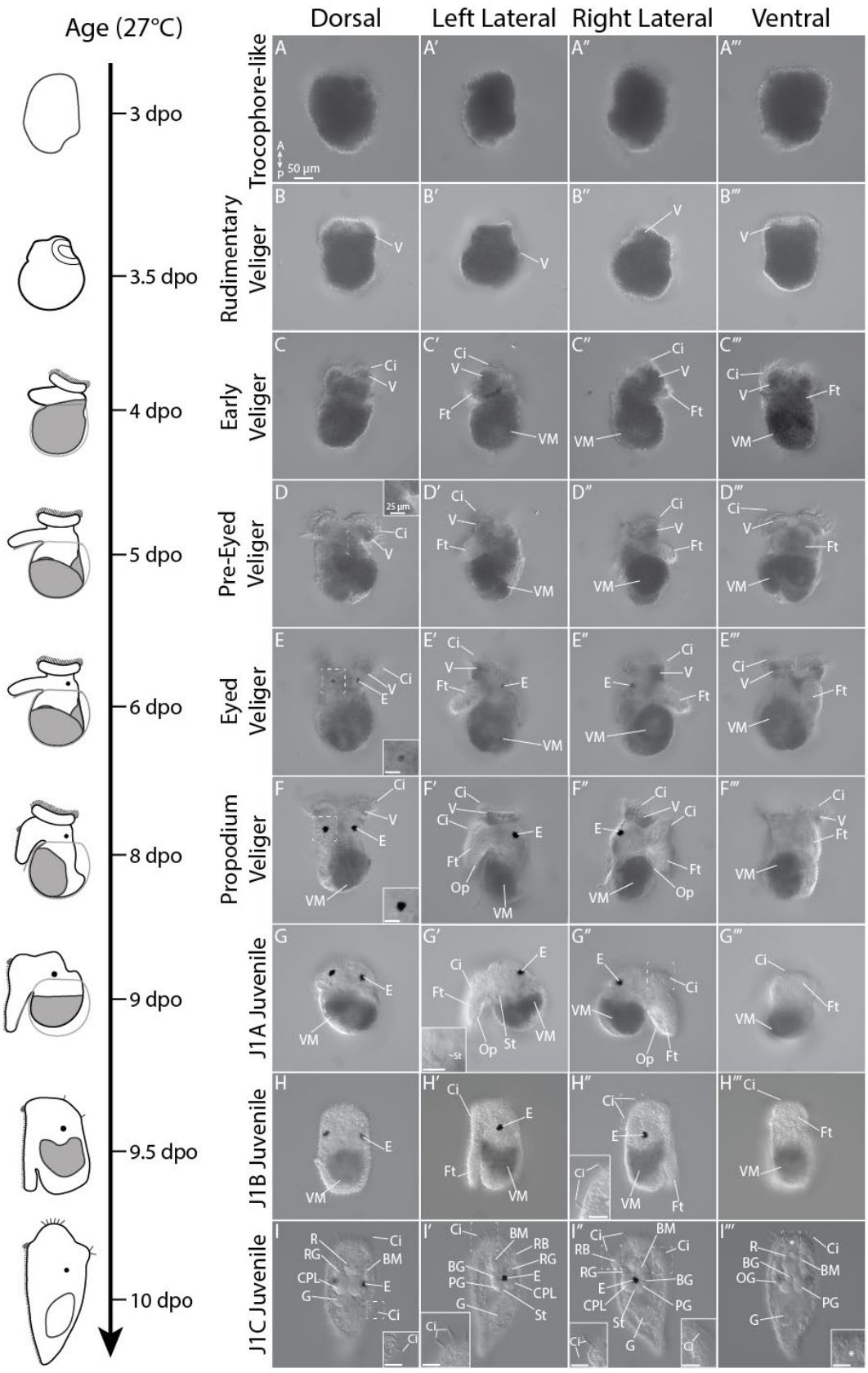
Age (27°C)
3 dpo
3.5 dpo
4 dpo
5 dpo
6 dpo
8 dpo
9 dpo
9.5 dpo
10 dpo
Dorsal
Left Lateral
Right Lateral
Ventral
Trocophore-like
Rudimentary Veliger
Early Veliger
Pre-Eyed Veliger
Eyed Veliger
Propodium Veliger
J1A Juvenile
J1B Juvenile
J1C Juvenile
50 µm
25 µm
A
P
V
Ci
Ft
VM
E
Op
St
BM
RB
RG
BG
PG
CPL
G
R
OG

One day later, the eyed veliger marks the first appearance of pigment associated with the eye (Figure 1.4, E Insert) at 6 dpo. Over time, this pigment becomes denser (Figure 1.4, F Insert). There are no noticeable changes to the velum, foot or visceral mass when compared to the pre-eyed veliger. At 8 dpo, the propodium veliger is defined by the presence of the propodium, an anterior growth of the foot that results in a “rounded” looking anterior end of the foot. The foot has also elongated and is now wrapped under the animal, forming almost an “L” shape. In addition to the propodium, the propodium veliger is easily staged due to the clustering of visceral mass on the right lateral side of the shell. The lobes of visceral mass cannot be distinguished as seen in earlier stages and is now clustered on the right lateral side (Figure 1.4, F).

Finally, the juvenile stage is reached when the shell and velum are lost (Figure 1.4, G), the animal has settled thus beginning crawling motility. The J1 juvenile has been subdivided into three distinct stages occurring after metamorphosis, which we name J1A, J1B, and J1C. This first juvenile stage is named stage 1A (J1A). The J1A stage is defined by the loss of the velum and shell, but retains the operculum. The foot has not changed significantly from the propodium veliger stage. At the J1B juvenile stage, the animal has lost the operculum and the visceral mass remains dorsal to the foot (Figure 1.4, H). Finally, the J1C juvenile can be identified due to its optical clarity, loss of visceral mass in favor of the gut, and presence of rhinophore buds (Figure 1.4, I). These rhinophore buds are the developing rhinophores, which begin to form at the dorsal

face of the animal and are marked by an elongated cilia tuft on the dorsal surface of each bud (Figure 1.4, I). After the J1C stage, the animal begins to feed and gradually elongates further, begins to develop the cerata, rhinophores, and oral tentacles further until reaching the adult stage.

CNS ganglia can be identified starting at the early veliger stage

The earliest stage where ganglia could be easily identified was the pre-eyed veliger. The cerebral (Figure 1.5, red), pedal (Figure 1.5, green), pleural (Figure 1.5, mustard), and visceral ganglia (Figure 1.5, dark red) were identifiable at this stage (Data not shown). The buccal ganglia, however, was identifiable at the next developmental stage, the pre-eyed veliger. (Figure 1.5, A & D) The CNS ganglia grow slightly in size through the last larval stage, the propodium veliger (Figure 3, G & K) but there are no significant changes in terms of ganglia position. Another landmark of metamorphosis is the merge of the cerebral and pleural ganglia. The J1A juvenile CNS consists of paired rhinophore, cerebropleural, buccal, and pedal ganglia. The single visceral ganglion is connected posteriorly to the left cerebropleural ganglion (Figure 1.5, H & L). Finally, at the J1C stage, the visceral ganglion merges with the left cerebropleural ganglion (Figure 1.5, J & N). The loss of the visceral ganglion marks the stage where the adult CNS has completely formed and there is a slight gap between the anterior end of the cerebropleural ganglia which form a “V” shape. At the J1B stage, this “V” shape has disappeared as the cerebropleural ganglia are now closer together.

Figure 1.5 CNS ganglia can be identified starting at the early veliger stage

Dorsal(A-G) and lateral (A'-G') views of DAPI staining from confocal microscopy for the Early Veliger to J1C Juvenile. Ganglia are highlighted for each stage. All scale bars are 50 μm. BG, Buccal Ganglion; CG, Cerebral Ganglion; CPL, Cerebropleural Ganglion; PG, Pedal Ganglion; Pl, Pleural Ganglion; RG, Rhinophore Ganglion; VG, Visceral Ganglion

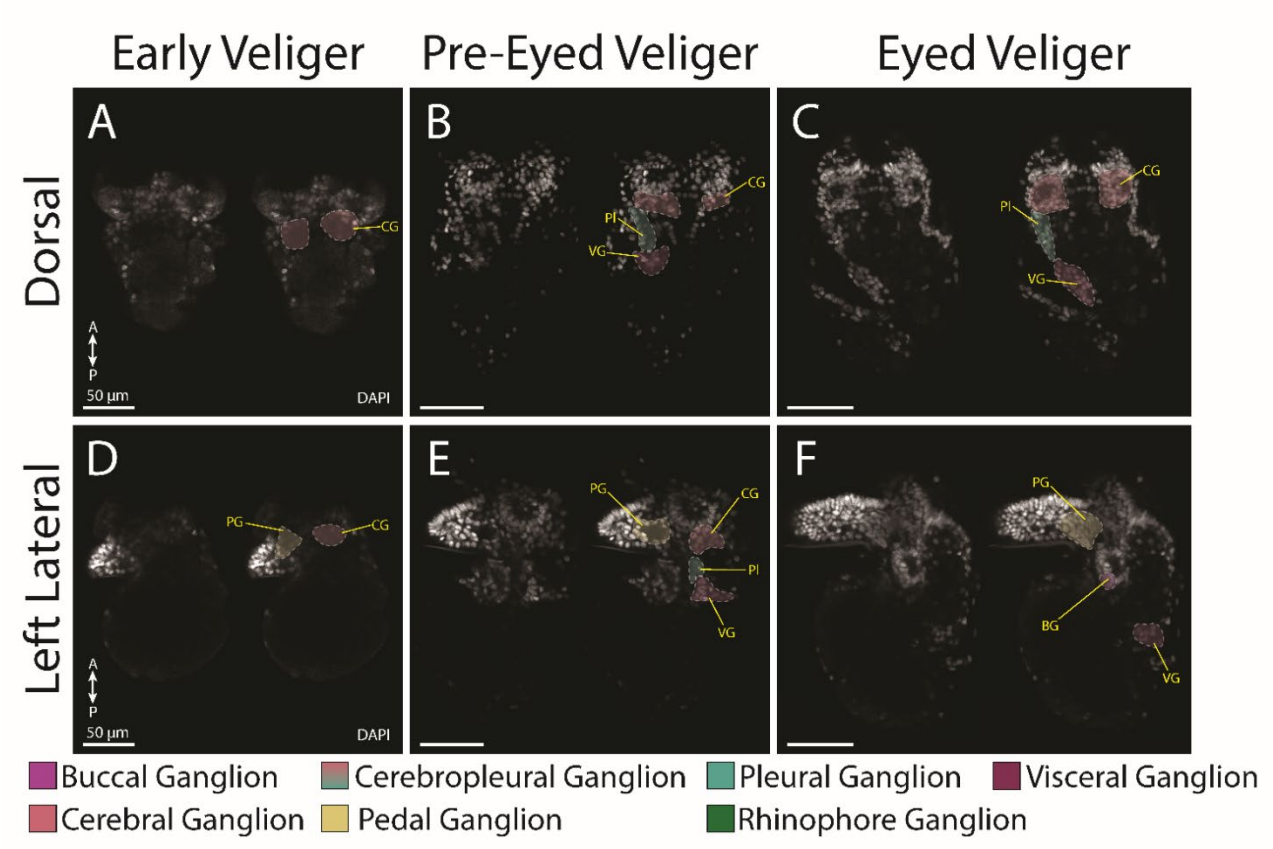
Early Veliger
Pre-Eyed Veliger
Eyed Veliger
Dorsal
Left Lateral
A
B
C
D
E
F
CG
PI
VG
PG
BG
A
P
50 µm
DAPI
Buccal Ganglion
Cerebropleural Ganglion
Pleural Ganglion
Visceral Ganglion
Cerebral Ganglion
Pedal Ganglion
Rhinophore Ganglion

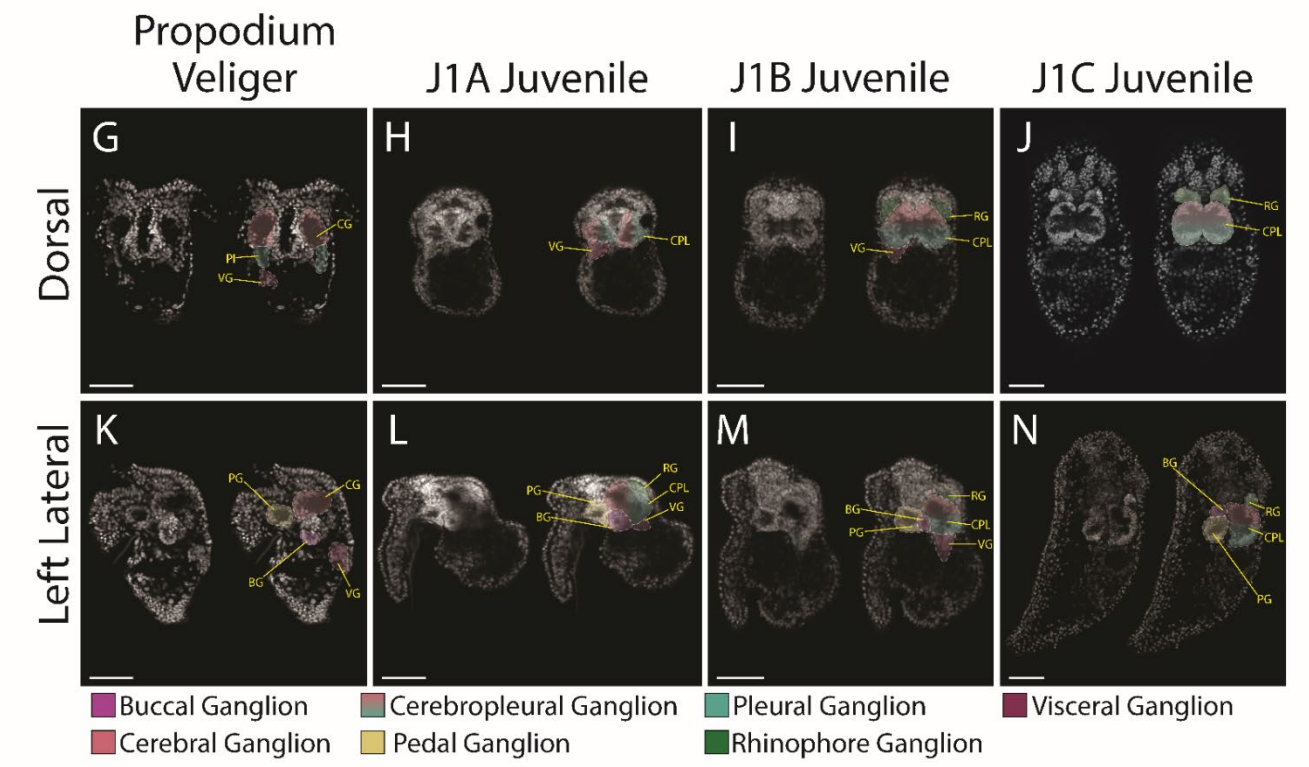
Propodium Veliger
J1A Juvenile
J1B Juvenile
J1C Juvenile
Dorsal
Left Lateral
G
H
I
J
K
L
M
N
CG
PI
VG
CPL
RG
PG
BG
Buccal Ganglion
Cerebropleural Ganglion
Pleural Ganglion
Visceral Ganglion
Cerebral Ganglion
Pedal Ganglion
Rhinophore Ganglion

The *Berghia* CNS undergoes changes in position and cell count during development

Throughout development, the CNS ganglia maintain a relatively consistent position in the animal throughout development. The most drastic change is the anterior movement of the buccal ganglia from posterior to the pedal ganglia to anterior of the pedal ganglia (Figure 1.6, A). Before metamorphosis, the ganglia are aligned with the dorsal pleural ganglia, but after metamorphosis the buccal ganglia are directly aligned with the pedal ganglia, located medial of the pedal ganglia. At the J1C stage, the buccal ganglia finally appear anterior of the pedal ganglia. This is hypothesized to occur due to the buccal ganglia's connection with the esophagus, which may move the ganglia as the animal elongates. During larval and juvenile stages, the CNS ganglia undergo positional and size changes due to metamorphosis (Figure 1.6, A). Despite the ganglia growth, the proportions of each ganglion have been maintained. This is supported by the cartoons traced from the CNS ganglia outlines (Figure 1.2). In order to quantify neuronal growth, the number of cells were counted in each ganglion at each developmental stage. A detailed description of the counting procedure can be found in Figure 1.2

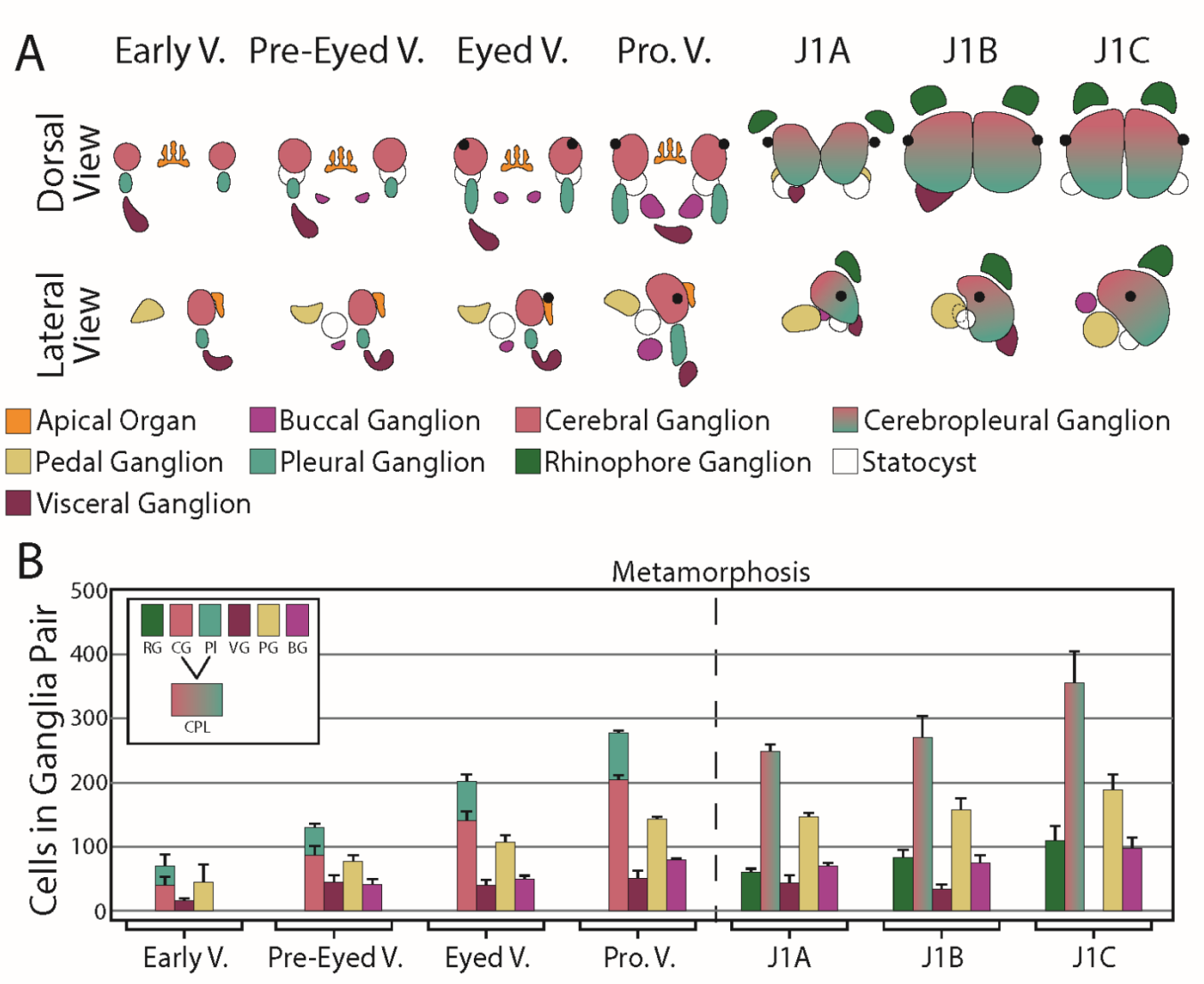

Figure 1.6 The Berghia CNS undergoes changes in position and cell count during development

(A) Ganglia cartoons for the early veliger through J1C juvenile. (B) Quantification of the number of cells in each ganglion between stages. The legend depicts the lateral order of the ganglia in the grouped bar chart. The cerebropleural ganglia is shown for stages where the cerebral and pleural ganglia are merged.

When quantified, it became clear that each ganglion grew at a different rate. (Figure 1.6, B). The cerebral and pleural ganglia follow a very interesting growth pattern. The ganglia both increase at a steady rate from the early veliger to the propodium veliger. However, after metamorphosis, the number of cells at the J1A juvenile in the combined cerebropleural ganglia seems decreased. The growth resumed again at the J1B and J1C stages, with a total of 356 ± 50 cells in the combined left and right cerebropleural ganglia at the J1C stage. Both the pedal and buccal ganglia grow consistently throughout development, ending at the J1C stage at 189 ± 25 cells in the pedal ganglia and 97 ± 19 cells in the buccal ganglia. The rhinophore ganglia appear after metamorphosis, first noted at the J1A stage totaling 60 ± 13 cells in the paired ganglia. At the J1C stage, the rhinophore ganglia had increased to 110 ± 24 cells. Finally, the visceral ganglion grew from the early veliger stage, beginning at 17 ± 4 cells, and 34 ± 9 cells at the J1B juvenile stage.

SCPb-*lir* and serotonin-*lir* in the CNS drastically changes after metamorphosis

After understanding and quantifying the growth of the central nervous system, the immunoreactivity patterns of SCPb-*like* and serotonin-*like* can now be qualitatively analyzed to confirm the morphological analysis of the CNS and describe how the CNS is affected by metamorphosis. Here, SCPb-*like* immunoreactivity (-*lir*) and serotonin-*lir* are described from the trochophore-like stage to the J1C juvenile stage. These two neurotransmitters were found to mark identifiable neurons in the adult brain (Figure 1.3, D). Thus, these markers can be directly compared between the larval, juvenile, and adult stages.

At the trochophore-like stage, there is no SCPb-*lir* or serotonin-*lir* (Figure 1.7, A & A'). The late trochophore-like stage marks the first presence of serotonin-*lir* and SCPb-*lir* immunoreactivity. seen at the margin of the forming shell gland (Figure 1.7, B' insert), and is present at the developing mantle edge until the eyed veliger stage. Initially, the mantle edge coexpresses SCPb-*lir* and Serotonin-*lir*, but SCPb-*lir* is lost after the early veliger stage. (Figure 1.7, E) Outside of the mantle edge immunoreactivity, the first immunoreactivity within the epithelium is seen at the rudimentary veliger stage. Two laterally paired SCPb-*lir* projections are seen along the epidermis of the body. (Figure 1.7, C insert) No soma could be distinctly connected to these projections. However, these PNS elements predate the CNS immunoreactivity, which forms at the early veliger stage. Serotonin-*lir* marks the apical organ, slightly anterior to the cerebral ganglia. The apical organ is seen from the early veliger until the propodium veliger and then lost at metamorphosis.

SCPb-*lir* commissures run between the cerebral ganglia, and projections run from each cerebral ganglia to their respective pedal, pleural and visceral ganglia.

The first immunoreactive cells are seen in and near the visceral ganglion (Figure 1.7, D). One cell is located on the epidermis (Figure 1.7, D, yellow wedge), near but not within the ganglion, while the other cell is located within the visceral ganglion (Figure 1.7, D, blue wedge). Both cells are connected to the ganglion from the cerebral ganglion projection. At the Eyed veliger stage, both of these cells are now found within the visceral ganglion. Additionally, SCPb-*lir* immunoreactivity is also seen in a small group of cells resembling a ganglion. This is only found on the left side of the body. Projections run from the left pleural ganglion down to this structure (Figure 1.7, E', F', & G' yellow arrow) and immunoreactive cells can be seen within. This structure is last seen at the propodium veliger stage and is lost after metamorphosis. Additionally, two faint SCPb-*lir* cells are seen anterior to the cerebral ganglion (Figure 1.7, G yellow wedge), cells also seen by (Ellis, 2010).

Figure 1.7 SCPb-lir and Serotonin-lir in the CNS drastically changes after metamorphosis

(A-J) Dorsal, (A'-J') lateral, and (G"-J") ventral views of DAPI, SCPb-*lir*, and Serotonin-*lir* throughout from the trochophore-like to the J1C juvenile stages. Ganglia are traced for each view. Image scale bars are 50 μm, insert scale bars are 25 μm. APO, Apical Organ

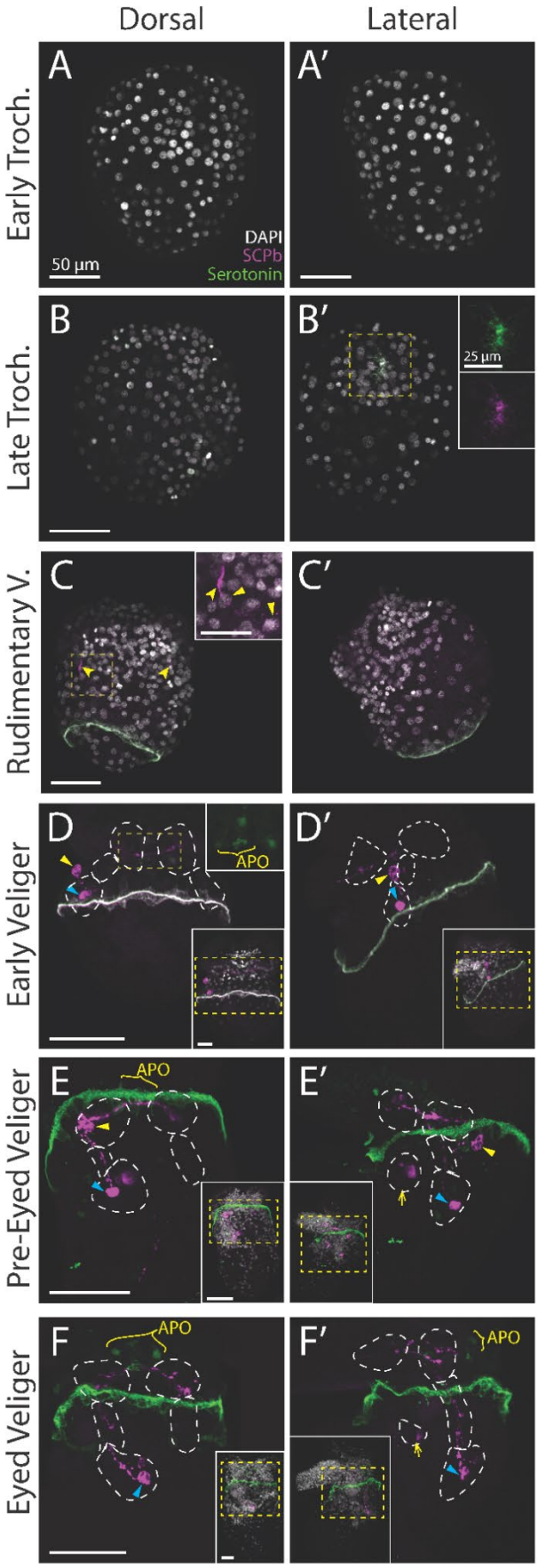
Dorsal
Lateral
Early Troch.
Late Troch.
Rudimentary V.
Early Veliger
Pre-Eyed Veliger
Eyed Veliger
A
A′
B
B′
C
C′
D
D′
E
E′
F
F′
DAPI
SCPb
Serotonin
50 µm
25 µm
APO

Figure 1.7 continued

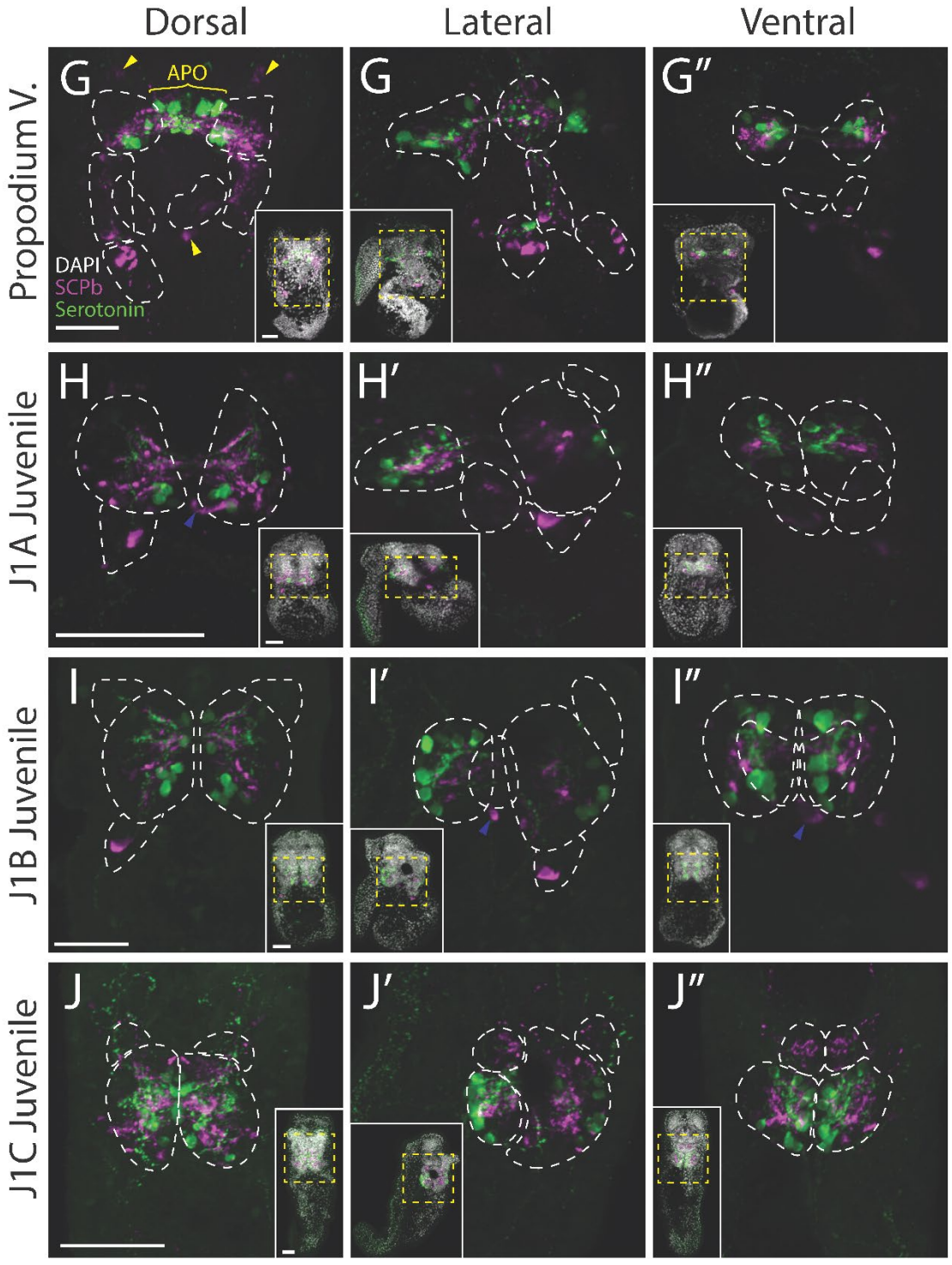

After metamorphosis, the rhinophore ganglia are innervated with SCPb-*lir* projections from the cerebropleural ganglia. Multiple commissures can be seen connecting the left and right cerebropleural spaced along the anterior posterior axis after metamorphosis (Figure 1.7, H-J). Between the J1B and J1C stages, the CNS changes very little, with the exception of the fusion of the visceral ganglion.

The visceral and left CPL ganglion merger at the J1C stage does not create cell count asymmetry

A single highly SCPb-*lir* cell is seen at the posterior tip of the visceral ganglion throughout the J1A and J1B stages (Figure 1.7, H-J, orange wedge). This cell appears to be one of the two strongly immunoreactive cells first formed at the eyed veliger stage, due to the strong immunoreactive signal, connection with projections from the pleural ganglion, and posterior location in the visceral ganglion. The neuropil connecting the visceral and left cerebropleural ganglia was used to confirm that the two ganglia are closely connected. Indeed, internally both SCPb-*lir* and serotonin-*lir* neuropil connect the left cerebropleural to the visceral ganglion (Figure 1.8, A). A singular immunoreactive cell marks the visceral ganglion at both the J1A and J1B stages. However, after the merge of the visceral ganglion at the J1C stage, a cell is seen at a similar location with similar neuropil projections (Figure 1.8, C). This suggests the identity of these cells is consistent and thus serves as confirmation of the merge of these ganglia. Interestingly, when comparing the number of cells in the left and right cerebropleural ganglia (Figure 1.8, D), there was no significant difference between them at any developmental stage. Despite the size of the visceral ganglion, these merged cells do not appear to create a statistically significant asymmetry between the left and right cerebropleural hemispheres despite a slight difference in average number of cells (Figure 1.8, D).

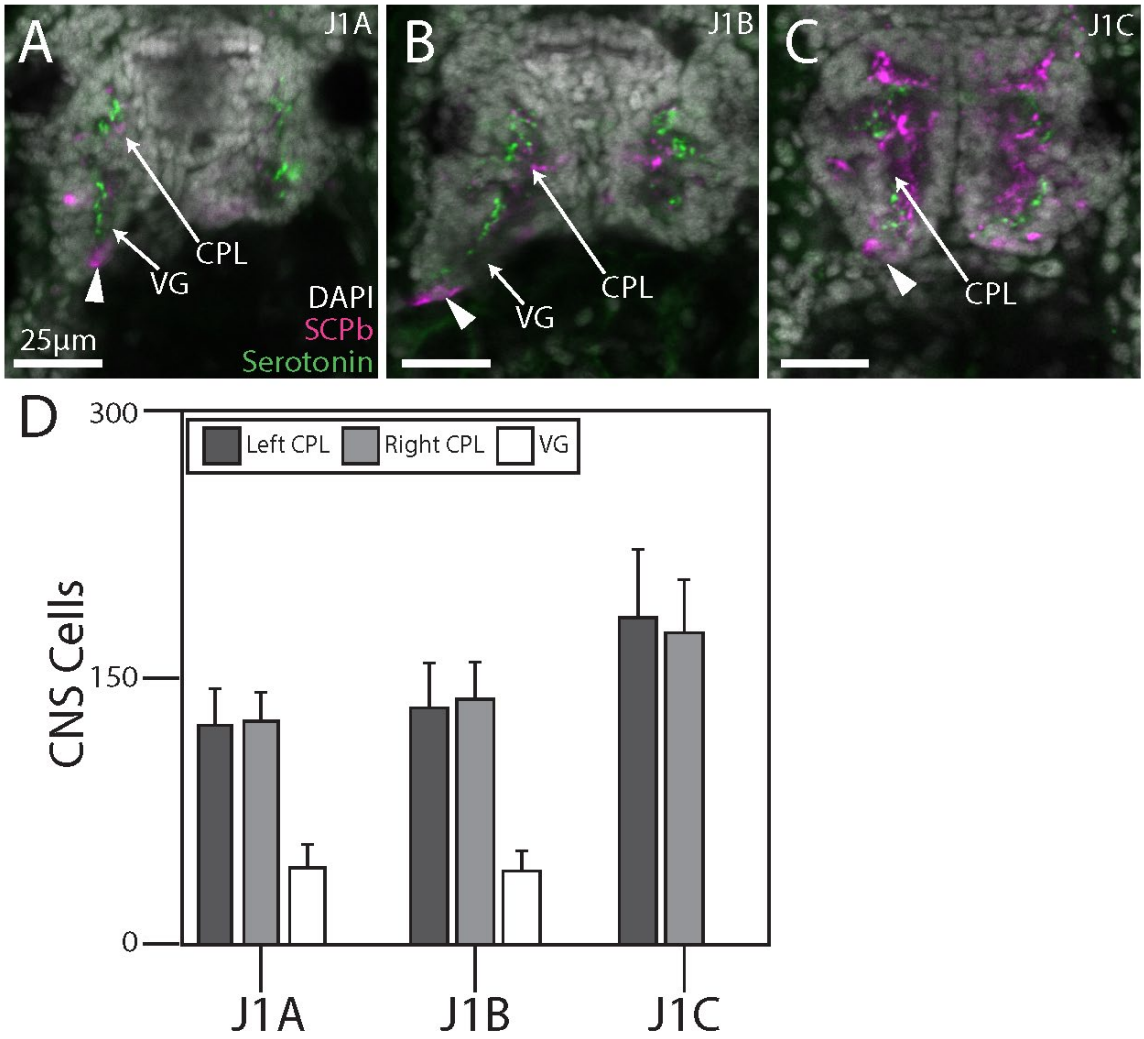

Figure 1.8 The visceral and left CPL ganglion merge at the J1C stage does not create cell count asymmetry

Dorsal views of the J1A juvenile (A), J1B Juvenile (B), and J1C Juvenile (C) cerebropleural ganglia. (D) Quantification of the cerebropleural and visceral ganglia cells at each stage. Each scale bar is 50 µm. CPL, Cerebropleural Ganglion; VG, Visceral Ganglion

SCPb-*like* and serotonin-*like* immunoreactive cells in the CNS grow rapidly immediately before and after metamorphosis.

Both serotonin-*lir* SCPb-*lir* cell counts seem to follow the same trend, despite no co-expression of SCPb and serotonin immunoreactivity. At the early veliger stage, there were on average 5.85 SCPb-*lir* cells and 3.67 serotonin cells. The number of cells increases slowly to 11.91 SCPb-*lir* cells and 5.61 serotonin cells at the pre-eyed stage. These cells roughly double at the eyed veliger stage, containing 9.66 SCPb-*lir* cells and 10.72 serotonin-*lir* cells. Between the eyed and propodium veliger stages, the number of immunoreactive cells increases rapidly to 35.32 SCPb-*lir* cells and 29.38 serotonin cells before slightly decreasing after metamorphosis at the J1A stage containing 34.45 SCPb-*lir* cells and 25.52 serotonin cells. The immunoreactive cell count barely increases between the J1B and J1C stages, at 47.12 SCPb-*lir* cells at both stages and 34.28 cells at the J1B stage and 34.40 serotonin-*lir* cells at the J1C stage.

The increase in the number of immunoreactive cells in the central nervous system does not match the increase of total cells in the central nervous system. The larval and juvenile *Berghia* brains at the studied stages appear to go through two distinct spikes at the propodium veliger and J1B juvenile stages despite a consistent growth of the central nervous system. The J1C stage retains an almost identical number of immunoreactive cells, despite a noticeable growth in total number of CNS cells.

When separated by ganglion, the immunoreactive cells in the CNS begin to specify within key ganglia while immunoreactive cells in other ganglia are eventually removed. For serotonin-*lir*, cells were first seen in the apical organ, but rapidly expanded to the cerebral, pleural, pedal, and buccal ganglia. After the rapid increase in the number of cells at the propodium veliger stage, serotonin-*lir* cells are almost exclusively found in the cerebral, pleural, pedal, and apical organ. After metamorphosis this expression pattern is retained; serotonin-*lir* cells are only found in the cerebropleural and pedal ganglia.

SCPb-*lir* cells are found in more ganglia both before and after metamorphosis. Before metamorphosis, SCPb-*lir* cells were located in every ganglion. At the propodium veliger stage, the number of immunoreactive neurons in the cerebral and pleural ganglia increased dramatically. However, after metamorphosis, some of these immunoreactive neurons were no longer found in the newly formed cerebropleural ganglia. Finally, at the J1C stage SCPb-*lir* cells were restricted to the cerebropleural, pedal, and buccal ganglia. Immunoreactive neurons were inconsistently detected in the rhinophore ganglia.

Figure 1.9 SCPb-like and Serotonin-like immunoreactive cells in the CNS grow rapidly immediately before and after metamorphosis.

(A) Quantification of total number of cells and immunoreactive cells from the trochophore-like stage to the J1C Juvenile. (B) Quantification of SCPb-*lir* cells in each ganglion between stages. (C) Quantification of serotonin-*lir* cells in each ganglion between stages. The gradient cerebropleural bar is shown for stages where the cerebral and pleural ganglia have merged. Error bars for all figures are standard deviation.

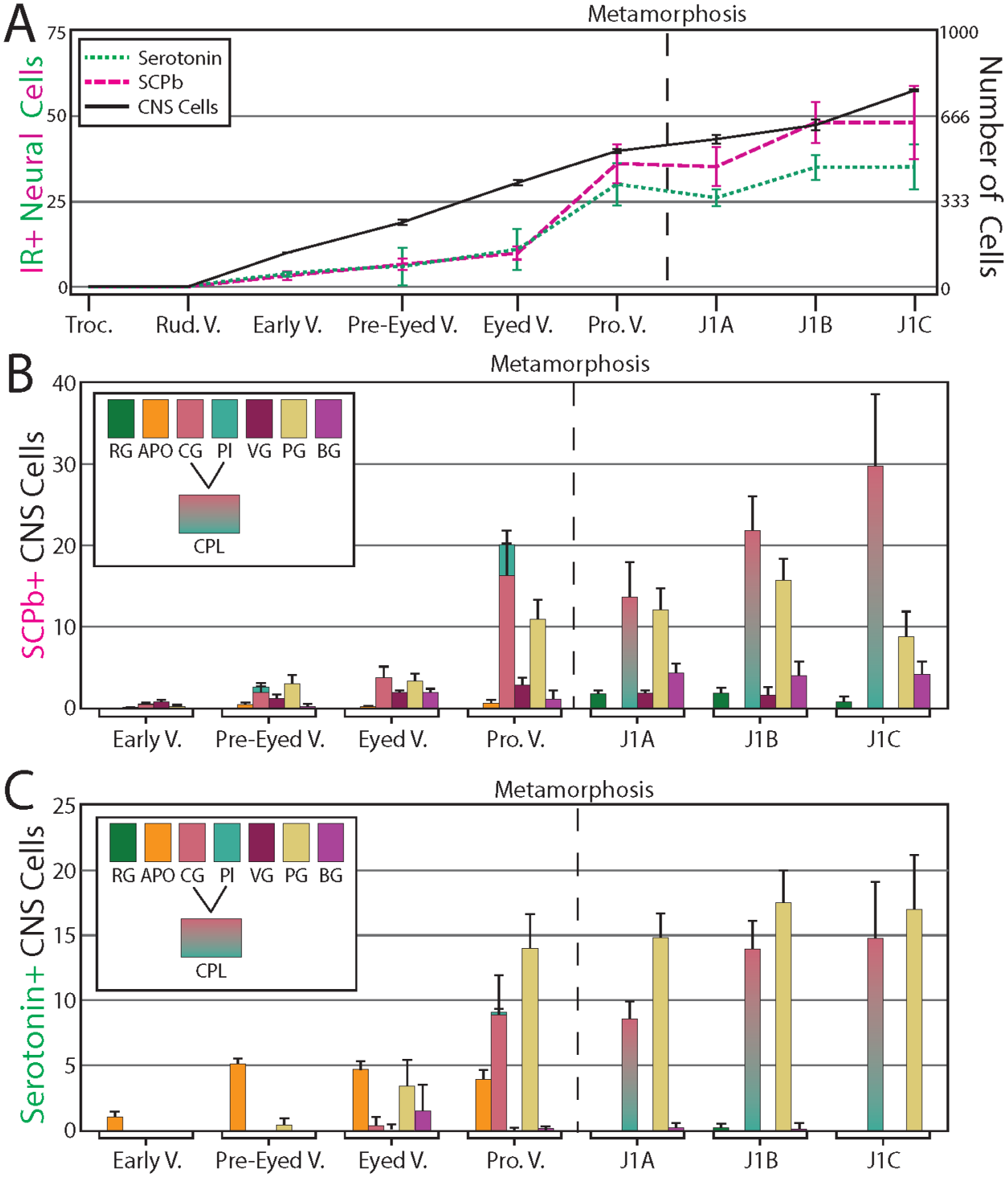
A
Metamorphosis
IR+ Neural Cells
Number of Cells
Serotonin
SCPb
CNS Cells
75
50
25
0
1000
666
333
0
Troc.
Rud. V.
Early V.
Pre-Eyed V.
Eyed V.
Pro. V.
J1A
J1B
J1C
B
Metamorphosis
SCPb+ CNS Cells
RG APO CG PI VG PG BG
CPL
40
30
20
10
0
Early V.
Pre-Eyed V.
Eyed V.
Pro. V.
J1A
J1B
J1C
C
Metamorphosis
Serotonin+ CNS Cells
RG APO CG PI VG PG BG
CPL
25
20
15
10
5
0
Early V.
Pre-Eyed V.
Eyed V.
Pro. V.
J1A
J1B
J1C

Serotonin-*like* immunoreactive cells can be identified in post-metamorphic stages

Unlike the adult CNS, identifiably large neurons are not obvious in juvenile stages. Despite the absence of these neurons, serotonin-*like* immunoreactivity patterns can still be traced and examined between animals and between the closely related juvenile stages due to the incredibly stereotyped CNS. In the three juvenile stages analyzed, six neuron identities were established by analyzing the position of serotonin-*lir* cells in the cerebropleural ganglia. The first cell identity, purple, is a clustered group of cells seen on the dorsal surface of the cerebropleural ganglia (Figure 1.10, A, C, E). At the J1A stage, an average of 3.82 ± 0.87 purple cells. At the J1B stage, there are now 4.27 ± 0.87 and finally 4.55 ± 0.93 cells. Another neuronal identity established at the J1A stage, the pink identity is a singular neuron on the right cerebropleural ganglion, towards the ventral surface in the middle of the ganglion (Figure 1.10, B). The pink neuron is only found in a subset of J1A juveniles and was not found at either the J1B or J1C stages. Additionally, the blue cell identity was found at all three stages, starting at the J1A stage. The blue cell identity was a single cell located at the posterior and ventral area of the cerebropleural ganglia (Figure 1.10, B, D, F). This cell buds off the connection between the right end of the pleural visceral loop and the posterior end of the right cerebropleural ganglion's neuropil.

After the J1A stage, the cyan and yellow paired cell identities were established at the J1B stage and are maintained at the J1C stage. Both of these

identities were singular paired cells found on the dorsal half of the ganglion and slightly anterior to the purple cell identity. They are laterally paired, but were sometimes found at slightly different locations when compared to each other (Figure 1.10, E). The yellow cell identity was found in 92% of animals at the J1B stage and 40.5% of J1C juveniles. The cyan cell identity was found in 50% of J1B juveniles and 64% of the J1C animals. Finally, the green cell identity are singular laterally paired cells that were found in every J1C animal analyzed (Figure 1.10, F). The green, cyan, and yellow cell identities are roughly vertically stacked at the J1B and J1C juvenile stages, with the yellow cells on top, cyan in the middle, and green on the ventral face of the ganglia (Figure 1.10, E & F). Notably, the green cell appears in the middle of the commissure between the cerebropleural ganglia, almost touching each other (Figure 1.10, F). Unfortunately, due to distinct morphological differences between the adult and juvenile cerebropleural ganglia, serotonin-*lir* cells could not be compared in this study.

Figure 1.10 Serotonin-like immunoreactive cells can be identified in post-metamorphic stages

The average location and amount of immunoreactive neurons in the brain of the settled veliger (A, A'), J1A juvenile (B, B'), J1B juvenile (C, C'), and adult (D, D'). The dorsal views are cut in half; (A-D) depict the dorsal to middle of the stack, and the middle to the bottom half are depicted by (A'-D'). Each dot represents the average position of a single cell based upon all replicates. Details can be seen in the below table.

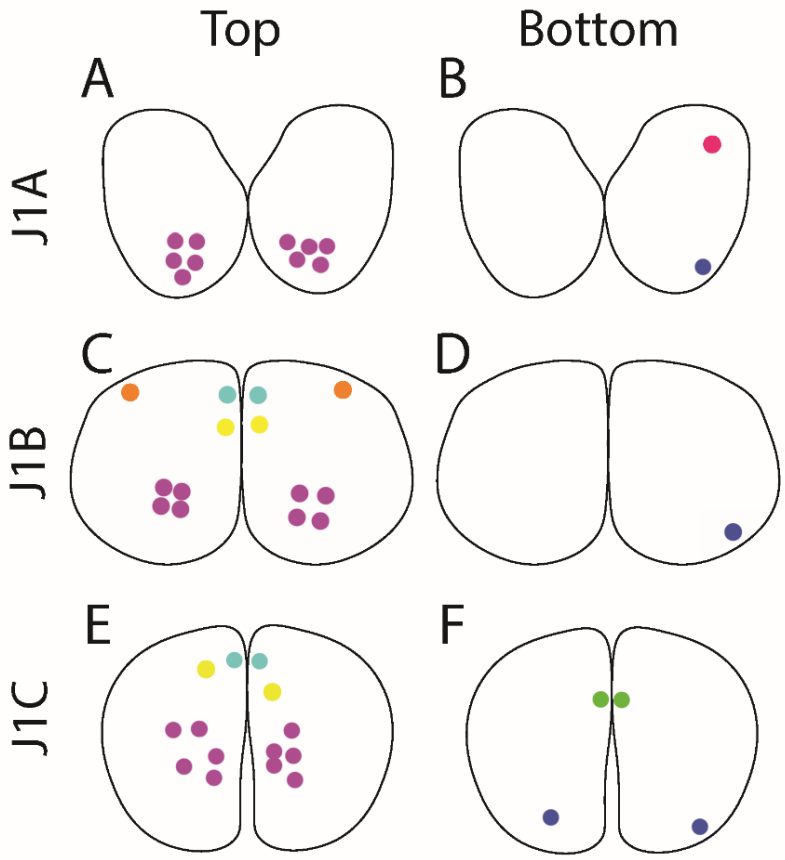

		J1A	J1B	J1C	Description
●	Left	3.82 ± 0.87	4.27 ± 0.87	4.55 ± 0.69	Tightly cluster of cells at the dorsal surface of the ganglion
	Right	3.82 ± 0.87	4.23 ± 0.57	4.55 ± 0.93	
●	Left	0.18 ± 0.40	0.47 ± 0.51	0.64 ± 0.50	Paired cells in the center of the ganglion, slightly anterior or below the yellow cells
	Right	0.18 ± 0.40	0.5 ± 0.51	0.64 ± 0.50	
●	Left	0.09 ± 0.30	0.93 ± 0.25	0.36 ± 0.50	Dorsal paired cells slightly anterior of the purple cells
	Right	0.09 ± 0.30	0.9 ± 0.31	0.45 ± 0.52	
●	Left	0.18 ± 0.40	0	1.00 ± 0.00	Ventral paired cells directly below the yellow and cyan cells
	Right	0.18 ± 0.40	0	1.00 ± 0.00	
●	Left	0	0	0	Singular, unpaired cell located near the ventral face of the ganglion.
	Right	0.27 ± 0.47	0	0	
●	Left	0	0.17 ± 0.38	0	Cell budding off the connection of the pleural visceral loop and right CPL neuropill
	Right	0	0.23 ± 0.43	0	
●	Left	0	0	0.18 ± 0.40	Cell budding off the connection of the pleural visceral loop and right CPL neuropill
	Right	0.73 ± 0.47	0.80 ± 0.41	0.73 ± 0.47	

Discussion

The CNS arises at the earliest veliger stages and reforms into the adult CNS after metamorphosis.

In order to describe when the process of metamorphosis in *Berghia* occurred, a 3-pronged evaluation was used based upon morphological, behavioral, and neuroanatomical features. The first criterion for identifying metamorphosis was the loss of the velum. The loss of the velum suggests the animal has transitioned from the swimming motility of the larval stage to the crawling motility of the juvenile stage. (Marois & Carew, 1990) (Bonar & Hadfield, 1974) Additionally, the oral tentacles arise from the same face as the velum. The loss of the velum clears the way for the development of the oral tentacles and the adult nervous system to support these organs. In *B. stephanieae*, the velum was lost at the J1A juvenile stage (Figure 1.4, G). The physical velum structure could no longer be seen and no cilia were noted using differential interference contrast microscopy.

The second criterion was the assumption of crawling motility. Animals that had settled and exclusively crawled suggests that in addition to the loss of the morphological features to support swimming motility, the animal had developed the neural circuitry to allow for crawling motility. (Marois & Carew, 1990) (Bonar & Hadfield, 1974) In *Berghia*, crawling motility was seen at the J1A stage as well. Some settled animals retained their shells but from observation were no

longer attached to the shells. A small proportion of animals settled while still retaining their velum. However, these animals also shed their velum and shells.

The final criterion was neuroanatomical rearrangement. Adapting the larval CNS into the post-metamorphic CNS marks drastic changes to neural circuitry, the behavior of the animal, and the innervation of the body. (Marois & Carew, 1990) (Carrol & Kempf, 1994) While difficult to resolve with differential interference contrast microscopy in post-metamorphic stages due to the density of visceral mass, with careful analysis it was possible to visualize the merged cerebropleural ganglia at the J1A juvenile stage. As studied in Carrol & Kempf, 1996, the cerebropleural ganglia was a strong indicator that the CNS had been transformed into the post-metamorphic state. Using these criteria, it is hypothesized that the propidium veliger marks the last stage analyzed before metamorphosis, and the J1A juvenile marks the first post-metamorphic stage.

Identified neurons can be found at post-metamorphic stages of *Berghia*

Prior to this study, identified neurons had only been detected in adult animals. The artificial limit to the adult stage was partially due to the lack of distinctly large identifiable neurons. This study has revealed that identified neurons can be discovered without the assistance of identifiable neurons using the stereotyped nature of the juvenile CNS ganglia. While neurons identified in the juvenile stages were unable to be located in adult animals due to the large gap of time in between the stages, these neurons are interesting even among the tightly grouped juvenile stages studied. Even within a 3 day time period after metamorphosis, some identified neurons appeared, while some disappeared between the J1A, J1B, and J1C stages. This suggests that studying identifiable neurons at this stage may provide information regarding the emergence of adult neural circuitry. It is not a far reach to imagine that the neural circuits found in adult stages, especially those responsible for crucial behaviors such as crawling or feeding, would form with the formation of the adult CNS ganglia. The ability to study this transformation of both morphology and behavior is unprecedented in gastropod neural research.

One of the most interesting results was the singular unpaired neuron, labeled as the “blue” neuron. This neuron was found on the right cerebropleural ganglion and was always attached to the pleural visceral loop. It is relatively uncommon in adult systems to identify an unpaired neuron, as identification criteria often rely upon parity due to the lack of morphological features outside of

the ganglia due to the dissection of the adult brain. One of the strengths of the juvenile model this study has established is the ability to collect and utilize information from the entire animal, as the brain can be imaged *in vivo* and does not require any dissection. These full animal mounts also allow for analysis of the PNS and the connections with the CNS.

PNS immunoreactivity arises before the CNS, which supports the forming CNS

The presence of laterally paired SCPb-*lir* neurons in the periphery that occur before the formation of the central nervous system aligns with previous literature in other gastropod species. This growing body of evidence suggests that these pre-CNS neurons play a role in guiding the formation of the future CNS. The specific mechanisms of this assistance are unknown, but these neurons are hypothesized to serve as pioneer neurons that the CNS use as guides to grow and connect ganglia with. The rapid disappearance of these neurons would align with this theory; when their role as pioneer neurons is no longer needed the neuron can be apoptosed. However, without more information regarding the function and nuclei associated with these neurons it is impossible to confirm the role of the PNS in *Berghia*.

The CNS anatomy of *Berghia* is settled

The CNS anatomy and developmental staging in existing *Berghia* literature has been confusing and inconsistent due to developmental asynchrony. Here, the development of a comprehensive morphology based staging system has solved the inconsistency in staging animals. Additionally, this study has settled the disputed CNS arrangement between Kristof & Klussman-Kolb, 2010 and Carrol & Kempf, 1996. We have confirmed the placement of the buccal ganglion as documented by Carrol & Kempf, but reject the presence of the visceral ganglion at the J1C stage documented by Carrol & Kempf, thus confirming the findings of Kristof & Klussman-Kolb. This study has also added a detailed atlas of *Berghia* development, both before and after metamorphosis. This atlas lays a solid foundation for future manipulation-based experiments, such as gene editing or physical manipulation of neurons, along with comparisons to the adult *Berghia* and to the larval and juvenile stages of other gastropods.

Merge of the VG and L CPL does not result in a significant L/R ganglion asymmetry

The merge of the visceral ganglion and the left cerebropleural ganglion after metamorphosis without creating an asymmetry between the left and right cerebropleural ganglia prompts questions regarding the mechanisms avoiding this asymmetry. While the exact mechanisms are unknown there are a few possible explanations. First, a portion of the visceral ganglion cells may be apoptosed during the merge. This explanation would account for the noticeable difference in mean number of cells not seen at previous stages. Then, the variation in number of cells between replicates would explain the lack of statistical significance. This theory is supported by the morphology of the left and right cerebropleural ganglia after the visceral ganglion merges. There is no obvious difference in shape or size between the two ganglia. However, a SCPb-*lir* cell at the posterior tip of the visceral ganglion appears at the posterior end of the newly merged left cerebropleural ganglion. If all 34 cells of the visceral ganglion were merged with the left cerebropleural to allow for the SCPb immunoreactive cell to maintain its posterior position, the density of cells in the left cerebropleural ganglion would be noticeably different.

Alternatively, the right cerebropleural ganglion may undergo a short period of rapid expansion between the J1B juvenile and the merge at the J1C juvenile stage to account for this difference. This theory too would account for the matching shape and size of the cerebropleural ganglia. However, this would suggest that the

right cerebropleural ganglion would be required to add around 20 cells more than the left cerebropleural ganglion between the J1B and J1C juveniles, or a 130% difference. Finally, the mechanisms at play may be a mix of both theories. Some of the visceral ganglion cells may be apoptosed to allow for the growth in the right cerebropleural to compensate for the smaller number of cells added to the left cerebropleural.

Conclusions

This study delineated a set of developmental stages from early development to post-metamorphosis, correcting for developmental temporal asymmetry that had harmed previous studies. These stages were then used with nuclear staining and immunohistochemistry to identify the CNS ganglia at each stage and analyze SCPb-*like* and serotonin-*like* immunoreactivity. The CNS ganglia were first identifiable at the early veliger stage. After metamorphosis, the rhinophore ganglia appear while the apical organ was lost and the cerebral and pleural ganglia merged. The merge of the visceral ganglion and the left cerebropleural ganglion was also identified, settling a debate within *Berghia* literature. Immunoreactivity patterns in the CNS were also analyzed for these developmental stages. Notably, two PNS neurons appeared before the formation of the CNS, which supported previous hypotheses in other gastropod molluscs suggesting the PNS plays a supporting role in CNS formation. Finally, serotonin-*like* reactive neurons were compared and consistently identified at post-metamorphic stages. These neurons were assigned identities and can be used as landmarks for future studies. This research has created an atlas of neural immunoreactivity and CNS ganglia growth for larval and juvenile stages in addition to mapping the first identified neurons in a non-adult gastropod.

Future Directions

Despite the ease of identifying neurons at the post-metamorphic J1A, J1B, and J1C developmental stages, these neurons could not be located in the adult stage of *Berghia stephanieae*. Further developing tracing tools such as lineage tracing or fluorescent proteins can allow for these key neurons to be tracked to the adult stage and finally identified in the adult animal. Additionally, attempting to trace the identified neurons at the juvenile stages backwards in development could provide evidence of the function of these neurons. If a neuron exists both before and after metamorphosis, the neuron most likely performs a function that is not affected due to the large behavioral changes occurring. This type of neuron would be more interesting, as the conserved function would likely remain conserved at the adult stage. Conversely, neurons that appear or disappear during metamorphosis may serve a stage-specific function. The paired nature of these neurons and CNS ganglia also may provide a convenient control for laser ablation or other manipulative experiments. Singular neurons can be targeted and both the behavior and development of experimental animals can be analyzed. Additionally, the lack of asymmetry after the merge of the visceral ganglion and the left cerebropleural ganglion brings interesting avenues of research around the mechanisms behind maintaining this symmetry. Finally, elucidating the role of the first PNS neurons would settle what, if any, role the peripheral nervous system plays in guiding the CNS formation.

Chapter 1, in part, is currently being prepared for submission for publication of the material. Whitesel, CA; Johnston, HT; Ramirez, MD; Katz, PS; Lyons, DC. The thesis author was the primary investigator and author of this material. Park Masterson of the Lyons Lab provided panel A of Figure 1.3. Dr. Desmond Ramirez provided panels B, C, and D of Figure 1.3.

Chapter 2: Studying the PNS in larval and juvenile *Berghia stephanieae*

Abstract

The CNS of the aeolid nudibranch *Berghia stephanieae* undergoes transformation during metamorphosis, resulting in the emergence of the adult CNS from the larval CNS. However, the PNS of *Berghia* has never been studied across metamorphosis and the innervation of sensory organs has not been studied. The use of a larval and juvenile model to study the PNS allows for an *in vivo* imaging approach, whereas the adult brain must be dissected prior to imaging due to the size of the animal. Using these smaller and younger animals allows for the PNS nerves seen at the adult stage to be connected with those nerves at juvenile stages. Thus, the innervation these nerves make in the juvenile can be applied to the adult *Berghia.* This study explores the immunoreactivity patterns of the neuropeptide small cardioactive peptide b (SCPb) and the neurotransmitter serotonin between the larval CNS and the juvenile CNS. It was found that the post-metamorphic juvenile is heavily innervated in the PNS. The foot, esophagus, and rhinophore were innervated with epidermal PNS neurons and nerve projections from the CNS. Finally, sets of elongated cilia with an apparent sensory function were identified as markers of the forming rhinophore and oral tentacle.

Introduction

Gastropods have commonly served as neural models due to the benefits of their distinct central nervous system. Identifiable neurons, neurons with larger than normal soma that serve as landmarks, and stereotyped CNS ganglia have made gastropods important sources of advancements in neurobiology and understanding the neural basis of behavior. Nudibranchs are especially interesting due to the presence of heavily innervated sensory structures, including the chemosensory rhinophores and the finger-like cerata that serve both defensive roles and as extensions of the digestive tract. However, in current gastropod neural models the brain must be dissected prior to imaging due to the amount of surrounding tissue. Thus, the positional information and projections of the CNS with respect to the PNS are lost in the adult. Using juvenile and larval models allows for imaging of the brain within the animal

Berghia stephanieae is an example of an excellent gastropod neural model due to the ease of culturing it in the lab, rapid embryo production, and creation of the larval and juvenile stage SCPb-*lir* and serotonin-*lir* neural atlases (Carrol & Kempf, 1994) (Figure 1.8). The neural development of the *Berghia* CNS has been studied. Before metamorphosis, the *Berghia* CNS consists of 8 ganglia. Paired cerebral and pleural ganglia are located on the dorsal face alongside the singular apical organ and the visceral ganglion. Ventral to these ganglia are the paired pedal and buccal ganglia. After metamorphosis, the apical organ is lost and shortly

afterwards the visceral ganglion is lost as well. Additionally, the cerebral ganglia fused with their respective pleural ganglia to form the cerebropleural ganglia.

Some neurons were consistently found at these developmental stages and were able to be identified, the first gastropod to have identified neurons established at non-adult stages. While the juvenile and larval stages of *B. stephanieae* lack distinct large soma to act as identifiable neurons, these stages benefit from the ability to image the CNS without removal by dissection. The ability to image the CNS within the animal allows for the whole animal to be examined. The CNS can be directly analyzed with respect to the PNS and the projections that connect the two. This can provide crucial information into the function of ganglia during development and confirm if the circuitry exists for the CNS to activate a certain behavior.

In nudibranch molluscs, serotonin is commonly used in neuroethological studies due to its influence on locomotion (Lewis, 2011) and the swim pattern generator circuit (Newcomb & Katz, 2008). Serotonin was found to directly induce animals to perform the swim behavior. When serotonin was introduced at a 10^{-4} M concentration of serotonin, all samples of the nudibranch *Tritonia diomedea* performed the swimming behavior (McGellan, 1994). Later it was discovered that serotonin directly modulates the swim pattern generator, the neural circuit underlying the predator avoidance behavior that some species of nudibranchs perform. At larval stages, serotonin is also a common marker of the apical organ

(Kempf, 1997). In *Berghia stephanieae* and other nudibranchs, the apical organ extends projections anteriorly and may play a role in sensing the stimulus at the velar lobes. (Kempf, 1997)

Small cardioactive peptide b (SCPb) is commonly used as a marker in gastropod molluscs due to consistent marking of a subset of identified neurons in multiple gastropods. SCPb plays an excitatory role in the heart (Wiens & Brownell, 1995) and more recently has been identified in an excitatory role for programs involved in feeding and locomotion such as esophageal contractions, swimming, and crawling behaviors (Watson, 2020). Both serotonin and SCPb play key roles in the central and peripheral nervous systems. However, the peripheral nervous system patterns of these neural markers have not been investigated in detail at non-adult stages. Leveraging the strengths of the juvenile and larval systems as neural models in *B. stephanieae*, this study is framed around two key questions:

- How does the gastropod PNS connect with the CNS throughout development?
- How does the PNS change during the metamorphic transition from the larval to juvenile stages?

How does the gastropod PNS connect with the CNS throughout development?

Gastropod nudibranchs undergo rearrangement of the CNS during metamorphosis as the larval CNS is further remodeled into the forming adult CNS. However, it is unclear for many gastropods if projections from the CNS into the PNS are maintained throughout metamorphosis or undergo a similar remodeling during metamorphosis. While the CNS may contain the neural circuitry responsible for the behavioral response, the PNS is responsible for passing the initiating sensory inputs and the output signal to generate the behavior. Understanding changes in the PNS can also provide evidence to the role of each CNS ganglion in *Berghia stephanieae*.

The PNS connections with the CNS have been investigated in non-nudibranch gastropods throughout development such as *Lymnea stagnalis* (Hegedűs, 2004) (Croll & Chiasson, 1989) and *Crassotrea gigas* (Ellis & Kempf, 2011). (Yurchenko, 2018) In nudibranchs however, PNS has been focused around the adult nudibranchs (Croll, 2003) or the larval apical organ. (Kempf, 1997) In adult nudibranchs, projections from the central nervous system have been identified and compared between species due to the stereotyped CNS ganglia and arrangement. In adult nudibranchs, there are generally 4 projections from each cerebropleural ganglia. One of these projections leads anteriorly to the rhinophore ganglion (Zaitseva, 2001) (Figure 1.3), two others also project anteriorly. The final projection runs posteriorly. There are 2 projections from the pedal ganglia, one

which projects anteriorly and the other projects horizontal to the pedal ganglion. (Newcomb, 2003) The number and location of projections has never been studied in juvenile nudibranchs.

Studies of the PNS at non-adult stages have focused on the apical organ and its function with respect to the peripheral nervous system. In *Berghia stephanieae*, studies have shown that the apical organ possesses serotonin-*lir* sensory dendrites that extend anteriorly into the velum. This study additionally identified serotonin-*lir* projections from the apical organ into each of the velum and also revealed heavy serotonin-*lir* innervation in the foot of the post-metamorphic J1C juvenile.

How does the PNS change during the metamorphic transition from larval to juvenile stages?

The peripheral nervous system also is responsible for innervating the body. During the transition from larval to the juvenile stage, the nudibranch will elongate rapidly. In order to cope with this elongation, metamorphosis must induce changes in the PNS to accommodate for rapid expansion. However, no PNS of a nudibranch neural model has been compared across metamorphosis before. Studying this metamorphic gap is crucial as it can provide insight into the sensory inputs that are received at each developmental stage. Then, these sensory inputs can provide clues about the behavior, ecology, and underlying neural circuitry.

Kempf et. Al, 1997 identified serotonin-*lir* projections from the apical organ into the velum and the pedal ganglion into the foot at 3 veliger stages. However, the resulting changes to the PNS after metamorphosis was never studied. During metamorphosis, the apical organ is lost in *B. stephanieae*. The fate of these projections and the reason for the density of serotonin-*lir* in the foot is unknown. Studies in another nudibranch, *Phestilla sibogae,* have revealed a complex web of innervation in the sensory organs at the adult stage along with several projections from the CNS. The origin of these projections is unknown. Additionally, it has been shown in multiple gastropods that the mantle edge and the shell gland found at the larval stage are highly innervated, and these neurons grow with the expanding mantle edge. While the exact function of these neurons is unknown, they are

thought to have a sensory function. This study explores the transition from the larval PNS to the juvenile PNS and identifies potential mechanisms within the juvenile PNS that allow for rapid elongation and growth of rhinophores, oral tentacles, and cerata. In this study, it was found that the post-metamorphic J1C juvenile had immunoreactive PNS elements concentrated in the foot and esophagus.

Methods

Embryo handling and immunohistochemistry

Adult *Berghia* were grown and egg masses handled as described in chapter 1. Embryos from these egg masses were handled and prepared for immunohistochemistry as described in chapter 1. Confocal microscopy images were processed in Image J and each animal's PNS projections were copied onto a cartoon version of the stage using Adobe Illustrator. Then, the PNS from each replicate was traced onto a cartoon of the animal. The PNS tracings were then characterized into distinct PNS elements and each cartoon was scored for these elements. These scores were used to create the average PNS for each developmental stage and a representative cartoon was created.

SEM Imaging

Embryos for SEM fixation were incubated with 7.5% MgCl2 in FSW for 30 minutes. The volume was then reduced to approximately 2mL and then an equal volume of 2% Osmium Tetroxide diluted in ultra-pure H_20 was added. Animals were fixed in the resulting 1% Osmium Tetroxide for 1 hour. Samples were washed with ultra-pure H_20 6 times over 2 days, stored at 4°C between washes, and then dehydrated in a 10%, 25%, 40%, 50%, 75%, 90%, 95%, and 99% series of 99% ethanol diluted in ultra-pure H_20. Then, animals were washed twice with 100% ethanol and dried with a molecular sieve for 10 minutes each while slowly rotating.

Afterwards, the ethanol was drained and replaced with HMDS through a series with concentrations of 25%, 50%, 75% and eventually 100% HMDS diluted in ethanol. Then, the samples were gently agitated to suspend animals in the tube and poured into a small petri dish and left to dry overnight with the lid slightly ajar. The dried animals were gently sprinkled onto the pin stub prepared with carbon tape and aluminum tape. A brush with an eyelash was used to gently orientate and stick loose samples to the stub. The samples were then sputter coated and imaged on a Zeiss EVO 10.

Detailed SEM fixation and imaging methodology

Specimens used for SEM fixation were relaxed using the same relaxation protocol as performed with immunohistochemistry fixation. After relaxation, specimens were moved to a 1.5 mL eppendorf tube. Specimens were then fixed by adding 4% Osmium Tetroxide diluted in DiH_2O to an equal volume of 1X PBS and 3.25% $MgCl_2$ for a final concentration of 2% Osmium Tetroxide for 1 hour rocking at RT. Osmium Tetroxide is incredibly toxic and all steps were performed in a fume hood. The specimens will turn black as a result of fixation. The entire tube may turn black if there are large amounts of microbes in the water. If this happens, change the eppendorf tube after 3 washes, as the tube will be stained black.

Over the course of 48 hours, specimens were washed 6 times with DiH_2O and stored at 4 C between washes. Waste must be disposed of in a waste container. Then, dehydrate the specimens to 99% EtOH in DiH_2O through a 10%, 25%, 40%, 50%, 75%, 90%, 95%, and 99% EtOH in DiH_2O series. Specimens were washed twice with 100% ethanol and dried with a molecular sieve for 10 minutes each while slowly rotating. The ethanol was drained and replaced with HMDS through a series with concentrations of 25%, 50%, 75% and eventually 100% HMDS diluted in ethanol. All HMDS steps were performed in a fume hood.Then, the specimens were gently agitated to suspend specimens in the tube and poured into a small petri dish. A notable percentage of specimens were lost at this step. A pasteur pipette was used to collect any remaining samples.

The specimens were left to slowly evaporate overnight with the lid slightly ajar in a fume hood. After evaporation, the dried animals were gently sprinkled onto a pin stub prepared with carbon tape with aluminum tape placed on top of it. Forceps were used to press the edge of the aluminum tape onto the carbon tape. The orientation of animals cannot be controlled. Good preparations will have large quantities of specimens. A brush with an eyelash was used to gently orientate and stick samples that had not fully attached to the stub. This brush was also used to collect any animals that step 9 did not remove from the dish. Samples had a tendency to “jump” off the stub when compressed with the eyelash. The samples were then sputter coated and imaged on a Zeiss EVO 10. Samples lasted approximately 3 months after sputter coating and could be reimaged multiple times.

Results

Summary of SCPb-*lir* and serotonin-*lir* in the CNS

At the trochophore stage, there is no SCPb-*like* or Serotonin-*like* immunoreactivity (Figure 2.1, A). Later, at the end of the trochophore stage, the beginning of the shell gland SCPb-*lir* and Serotonin-*lir* is seen. The rudimentary veliger marks the first SCPb-*lir* immunoreactivity outside of the shell gland. Two paired immunoreactive projections run down the lateral faces of the body. Located in the epithelial layers, these projections appear to be part of the peripheral nervous system (Figure 2.1, B). However, no cell body could be clearly associated with these projections. At the early veliger stage, the cerebral ganglia, pleural ganglia, and pedal ganglia pairs in addition to the singular visceral ganglion and apical organ were first identified. Each ganglion also expresses SCPb-*lir* with the cerebral ganglia having an SCPb-*lir* commissure between the paired ganglia. The apical organ contains both SCPb-*lir* and serotonin-*lir* at this stage (Figure 2.1, C). At the pre-eyed veliger stage (Figure 2.1, D) the cerebral commissure permanently gains serotonin-*lir* in addition to pre-existing SCPb-*lir*. Additionally, SCPb-*lir* is lost in the apical organ. Later at the eyed veliger stage, the first buccal ganglion immunoreactivity and loss of serotonin-*lir* from the pleural and visceral ganglia (Figure 2.1, E). At the final larval stage, the propodium veliger, two faintly SCPb positive cells were located slightly anterior of the cerebral ganglia, near the velum (Figure 2.1, F). These cells had been noted during *Berghia* development (Ellis,

2010) and serve as a great metric to calibrate staging systems using a distinct immunoreactive marker.

After metamorphosis, serotonin projections connect the cerebropleural ganglia to the rhinophore ganglia at the J1A juvenile stage. Additionally, the pleural-visceral loop runs internally from the left cerebropleural, through the visceral ganglion and into the right cerebropleural ganglion. Finally, a uniquely comma shaped SCPb positive cell was noticeably elongated beyond the right cerebropleural ganglion with no known projection (Figure 2.1, G). After the merge of the visceral ganglion and left cerebropleural ganglion at the J1C juvenile stage, the serotonin-*lir* loop connects both ganglia (Figure 2.1, I).

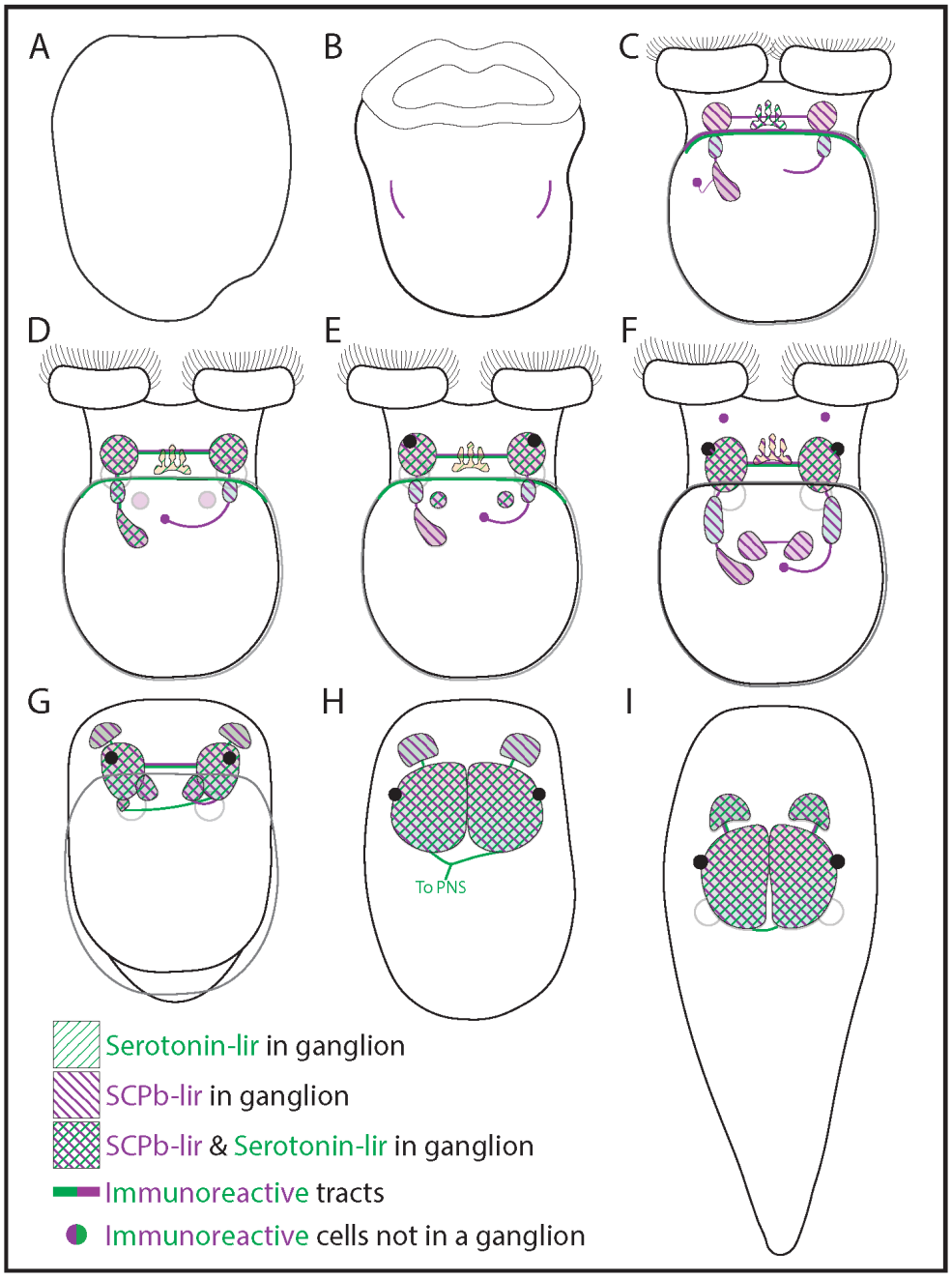

Figure 2.1 Summary of SCPb-lir and Serotonin-lir in the CNS
Confocal microscopy of DAPI, phalloidin and acetylated α-Tubulin-*lir* from the eyed veliger to the J3 juvenile stage. Image scale bars are 50 μm, insert scale bars are 25 μm. LRM, Larval Retractor Muscle; L. Mus, Longitudinal Muscle; Ci, Cilia; Ci Tuft, Cilia Tuft; Vt. tuft, Ventral Tuft; Rh. bud, Rhinophore Bud

Elongated cilia are found at the sight of future rhinophores and oral tentacles

At the eyed veliger stage, phalloidin counterstaining highlights the elongated larval retractor muscle (LRM) which runs from the velum to the posterior end of the shell (Figure 2.2, B). Later at the propodium veliger stage, there is a slight curve to the posterior end of the muscle, which is attached closer to the right lateral face (Figure 2.2, E). At the J1A juvenile, the larval retractor muscle is present but has drastically decayed. Its remnants are attached to the right lateral face of the posterior region (Figure 2.2, H). At the J1B and J1C juveniles, the LRM is completely lost and replaced by the juvenile musculature (Figure 2.2, K & N).

At the eyed and propodium veliger stages, the velum are heavily ciliated and a small tuft of cilia is seen at the left lateral side of the animal at the propodium veliger stage (Figure 2.2, C & F). After metamorphosis, at the J1A Juvenile stage, the ciliated velum are no longer seen; confirming the loss of the velum (Figure 2.2, H). Later, at the J1B Juvenile stage, there are tufts of cilia scattered on the lateral and dorsal faces of the body (Figure 2.2, L). On the dorsoanterior face of the animal, elongated cilia can be seen, predating the formation of any sensory structure (Figure 2.2, L insert). Later at the J1C stage, these cilia have elongated significantly. These cilia are found at the sites of the forming rhinophore buds and oral tentacles. After the rhinophores and oral tentacles have developed further, the J13 stage retains these distinctly large cilia at the rhinophores and oral tentacles (Figure 2.2, U, yellow arrow).

Figure 2.2 Elongated cilia are found at the sight of the future rhinophore and oral tentacles

Confocal microscopy of DAPI, phalloidin and acetylated α-Tubulin-*lir* from the eyed veliger to the J3 juvenile stage. Image scale bars are 50 μm, insert scale bars are 25 μm. LRM, Larval Retractor Muscle; L. Mus, Longitudinal Muscle; Ci, Cilia; Ci Tuft, Cilia Tuft; Vt. tuft, Ventral Tuft; Rh. bud, Rhinophore Bud

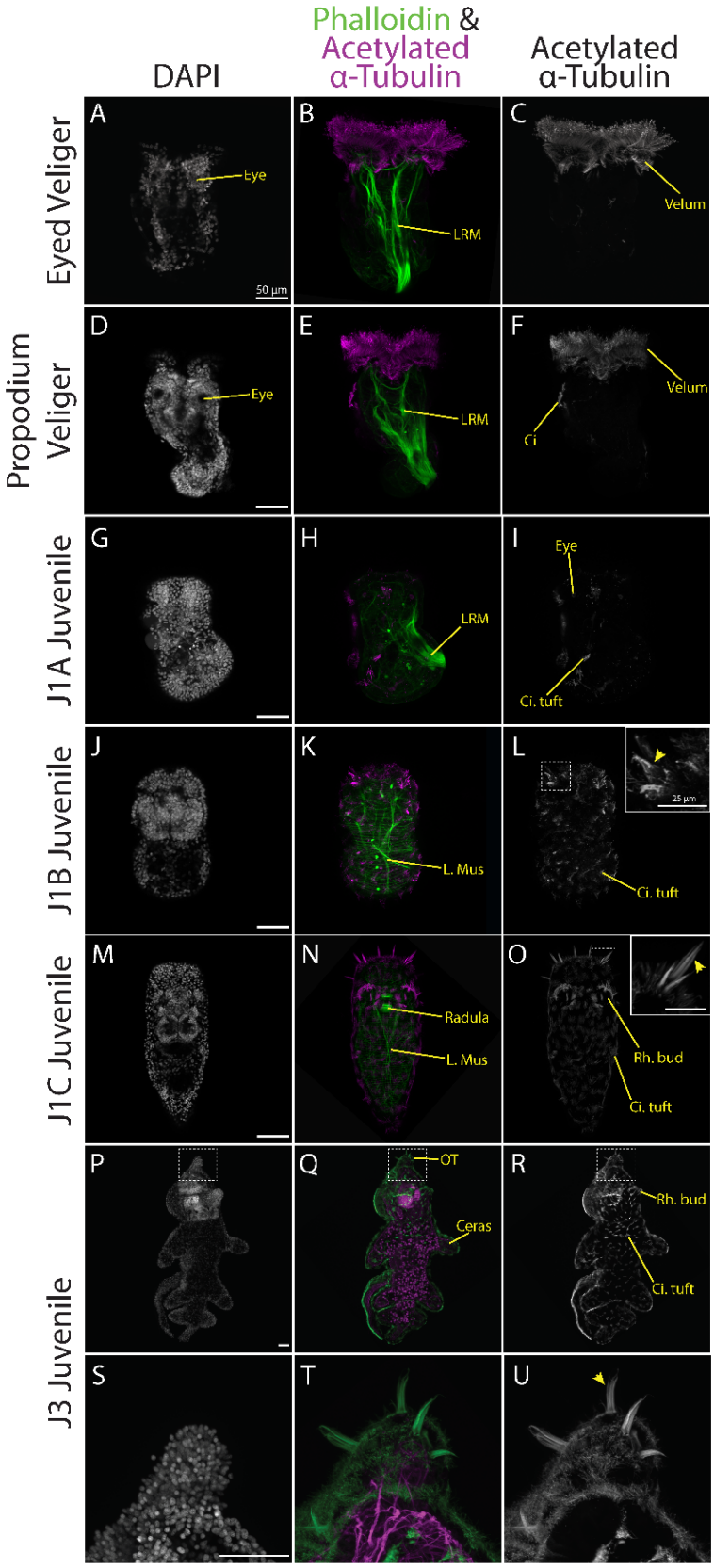
DAPI
Phalloidin & Acetylated α-Tubulin
Acetylated α-Tubulin
Propodium Veliger
Eyed Veliger
J1A Juvenile
J1B Juvenile
J1C Juvenile
J3 Juvenile
A
B
C
D
E
F
G
H
I
J
K
L
M
N
O
P
Q
R
S
T
U
Eye
LRM
Velum
Ci
Ci. tuft
L. Mus
Radula
Rh. bud
OT
Ceras
50 µm
25 µm

Elongated cilia seen at the forming sensory organs are tightly bound groups of cilia

After metamorphosis, at the J1A juvenile stage, the shell has been lost. However, at this stage the operculum remains (Figure 2.3, A). Cilia tufts can be seen over the entire body as seen with α-tubulin immunoreactivity (Figure 2.3, A). Also at the J1A stage, the rhinophore buds begin to form (Figure 2.3, A yellow arrows) where the future rhinophore will be. However, no long cilia are seen at the rhinophore buds. At the J1B stage, the rhinophore buds are more pronounced and long cilia can be seen at both the rhinophore buds (yellow arrows) and on the anterior face (green arrows) where the future oral tentacles will form (Figure 2.3, B-D). Finally, at the J1C stage (Figure 2.3, E-F), the rhinophores are more pronounced on the anterior face. A large cilia tuft at the anterior end of the foot can also be seen. The elongated cilia on the rhinophore and anterior face have grown in length as seen with α-tubulin immunoreactivity (Figure 2.3, E-F). Each rhinophore contains multiple cilia that point in different directions. These cilia are only found at the site of the rhinophores and oral tentacles and identified by both α-tubulin immunoreactivity and SEM could be linked to the juvenile PNS.

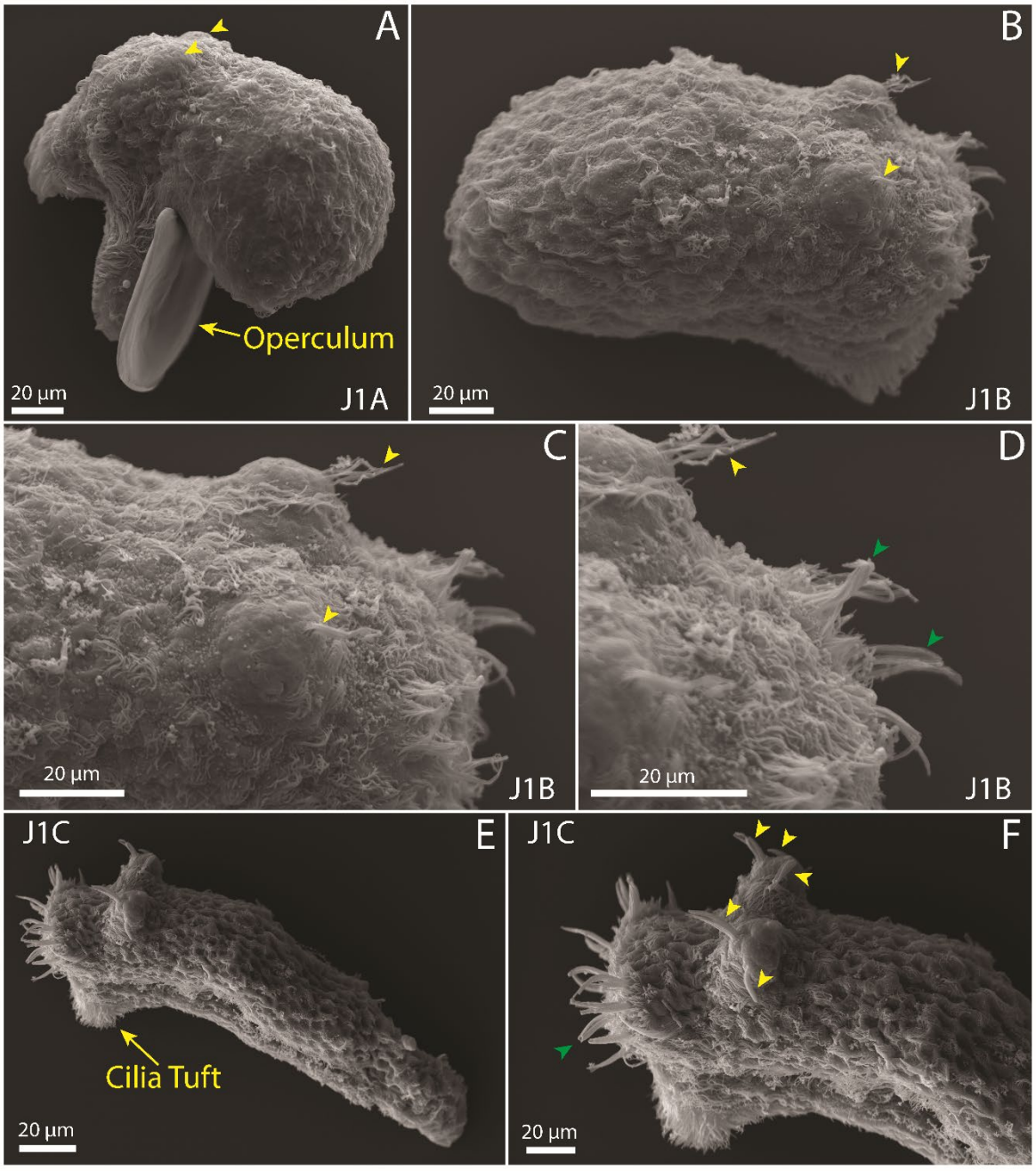

Figure 2.3 Cilia seen at the forming sensory organs with SEM

Scanning electron microscopy of J1A (A), J1B (B-D), and J1C (E, F) juveniles. Image scale bars are 20 µm.

SCPb-*lir* in the PNS expands after metamorphosis

At the Eyed Veliger stage, there was variable SCPb-*lir* in the peripheral nervous system found in a minority of animals. 3 patterns were found at this stage and were found in varying combinations in a minority of analyzed animals. First, immunoreactivity within the visceral mass (Figure 2.4, A, red arrow) was seen in projections of varying lengths and positions. Secondly, some animals displayed a projection from the right pleural ganglion which ended in an immunoreactive cell body located slightly lateral to the visceral ganglion (Figure 2.4, A, orange arrow). Finally, another subset of animals had a paired projection extending anteriorly from the cerebral ganglion ending in an immunoreactive cell near the velum (Figure 2.4, C & D). Notably, all animals with these anterior projections did not have the standard serotonin-*lir*.

After metamorphosis at the J1C stage, the amount of SCPb-*lir* in the PNS from the pedal and cerebropleural ganglia had expanded significantly. First, there was consistent immunoreactivity around the exterior of the gut. Next, two laterally paired projections extend anteriorly from the cerebropleural ganglia and connect with a short projection from the buccal ganglion. These projections terminate at the esophagus and radula (Figure 2.4, E & F, pink arrows). Laterally paired projections from the PG also extend anteriorly (Figure 2.4, D, blue arrows), but these projections appear to innervate the anterior end of the foot. Extending posteriorly from the CPL is two laterally paired projections (Figure 2.4, E & F, green arrows)

that track dorsal to the gut, following the downwards sloping ectoderm and terminating at the posterior end of the foot. Also terminating at this point is a paired projection from the PG which is ventral to the gut, close to the foot. These three projections meet at the posterior end of the foot. These patterns were consistently found in animals analyzed, unlike the veliger PNS.

Figure 2.4 SCPb-*like* immunoreactivity in the PNS expands after metamorphosis.

Confocal microscopy of SCPb-*like* immunoreactivity in the eyed veliger and J1C juvenile in dorsal (A, C) and lateral (B, D) views. All scale bars are 50 μm. APO, Apical Organ; BG, Buccal Ganglion; CG, Cerebral Ganglion; CPL, Cerebropleural Ganglion; PG, Pedal Ganglion; Pl, Pleural Ganglion; VG, Visceral Ganglion

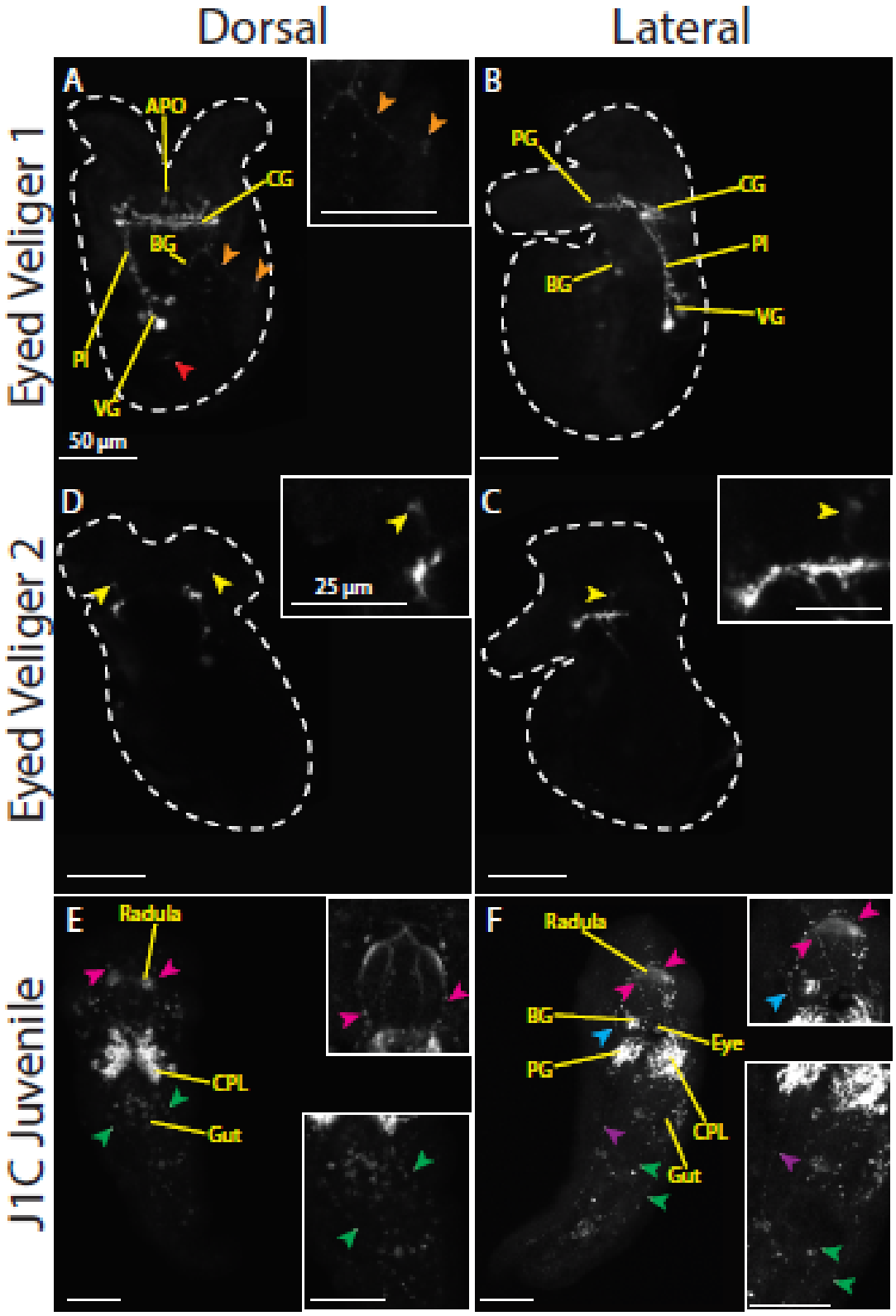
Dorsal
Lateral
Eyed Veliger 1
Eyed Veliger 2
J1C Juvenile
A
APO
CG
BG
PI
VG
50 µm
B
PG
CG
PI
BG
VG
D
25 µm
C
E
Radula
CPL
Gut
F
Radula
BG
Eye
PG
CPL
Gut

Serotonin-*lir* in the post-metamorphic juvenile extensively marks the foot

Serotonin-*lir* patterns at the eyed veliger stage are more consistent than SCPb-*lir* at this stage. Most noticeably, the developing mantle edge, which marks the edge of the developing shell, is strongly marked by serotonin-*lir* in these cell bodies (Figure 2.5, A & B, orange arrow). The only other PNS elements project from the flask-shaped cells of the apical organ. The flask cells to the left and right of the center cell project anteriorly towards the epidermis between the velum. Then, this projection branches towards the respective velum at a near right angle (Figure 2.5, A & B, yellow arrow). Finally, a large majority of eyed veligers analyzed had a projection from each pedal ganglion into the foot.

After metamorphosis, the apical organ is lost along with the PNS projections from it. However, serotonin-*lir* projecting from the pedal and cerebropleural ganglia has formed in the absence of the apical organ. First, the foot epidermis is heavily innervated, forming a web of neurons (Figure 2.5, D, yellow bracket). Innervating this foot are two projections from the cerebropleural ganglia and three from the pedal ganglia. The two cerebropleural projections extend from the posterior end of the foot dorsal to the gut and follow the downwards curve of the posterior epidermis. These projections end at the posterior end of the foot and connect with a posterior pedal ganglia projection (Figure 2.5, C & D, green arrow). The pedal ganglia project one paired nerve to the anterior part of the foot (Figure 2.5, D, blue arrow). Secondly, two paired

projections extend ventrally into the center of the foot. (Figure 2.5, D, orange arrow) Finally, a large nerve runs posteriorly to the posterior end of the foot and is positioned ventral to the gut (Figure 2.5, D, purple arrow). Along the way, several branches drop to the ventral foot. (Figure 2.5, D, small purple wedge) In addition to the foot immunoreactivity, two sets of paired projections extending anteriorly from the CPL to the buccal mass and esophagus were seen in a minority of animals (Figure 2.5, C & D, pink arrow). Finally, most animals had innervation in the epidermis of the rhinophore bud.

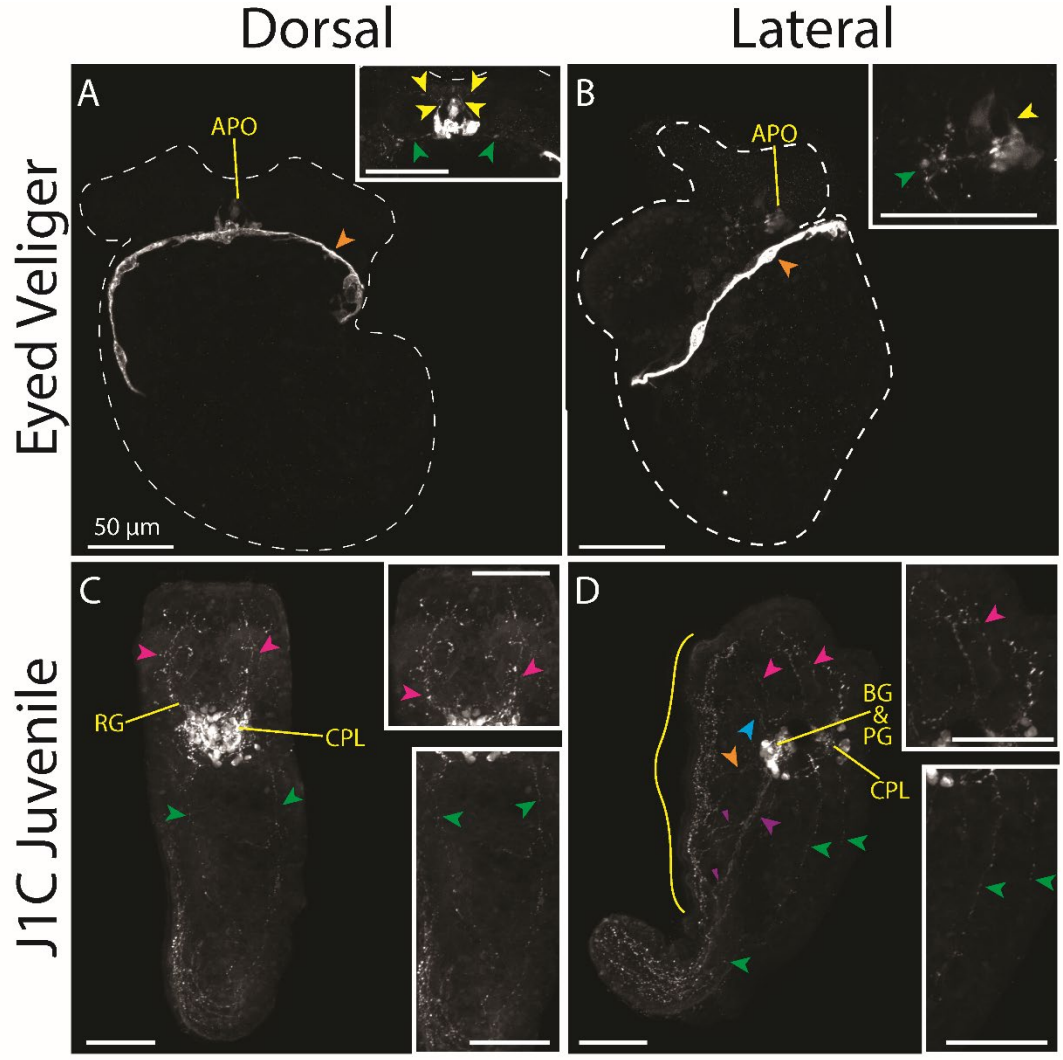

Figure 2.5 Serotonin-lir in the post-metamorphic juvenile extensively marks the foot.

Confocal microscopy of serotonin-*like* immunoreactivity in the eyed veliger and J1C juvenile in dorsal (A, C) and lateral (B, D) views. All scale bars are 50 µm. APO, Apical Organ; BG, Buccal Ganglion; CG, Cerebral Ganglion; CPL, Cerebropleural Ganglion; PG, Pedal Ganglion; RG, Rhinophore Ganglion

Summary of PNS SCPb-*like* and serotonin-*like* immunoreactivity

SCPb-*lir* in the eyed veliger was inconsistent. Most animals had no immunoreactivity, but small portions had patches of immunoreactivity in the visceral mass, projections from the right pleural ganglia, or paired projections from the anterior end of the cerebral ganglia and ending with an immunoreactive cell body (Figure 2.6, B & E). After metamorphosis, SCPb-*lir* was seen in the gut, projections from the cerebropleural into the esophagus and buccal mass, and projections into the foot from the cerebropleural ganglia and pedal ganglia (Figure 2.6, H & K). Unlike SCPb-*lir*, Serotonin-*lir* in the pre-metamorphic PNS is limited to a small number of features: the apical organ, pedal ganglia projection, and mantle edge tissue (Figure 2.6, A & D). However, after metamorphosis, the immunoreactivity patterns expand immensely. The foot is laced with a web of serotonin-*lir* neurons. 5 paired projections from the cerebropleural and pedal ganglia innervate the foot from anterior to posterior. Additionally, each of these projections branch before they connect with the foot. Some inconsistent immunoreactivity was seen in neurons branching anteriorly from the cerebral ganglia to the buccal mass and esophagus. Finally, the rhinophore buds were innervated in most animals (Figure 2.6, G & J).

Some of these projections appear to coexpress SCP-*like* and serotonin-*like* immunoreactivity. First, the anterior projection from the pedal ganglion into the foot appears to coexpress both neurotransmitters. However, SCPb-*lir* is not seen in the

branches between the main projection and the foot (Figure 2.6, I & L). This trend is also seen in the posterior projection from the pedal ganglia. SCPb-*lir* is limited to the main nerve while serotonin-*lir* is found in the main nerve and its branches (Figure 2.6, I & L). The final nerves are those extending from the posterior end of the cerebropleural ganglia and into the posterior end of the foot (Figure 2.6, I & L).

Figure 2.6 Summary of PNS SCPb-like and Serotonin-like immunoreactivity

Cartoon depictions of the average eyed veliger and J1C juvenile SCPb-*lir* and serotonin-*lir* in the PNS.

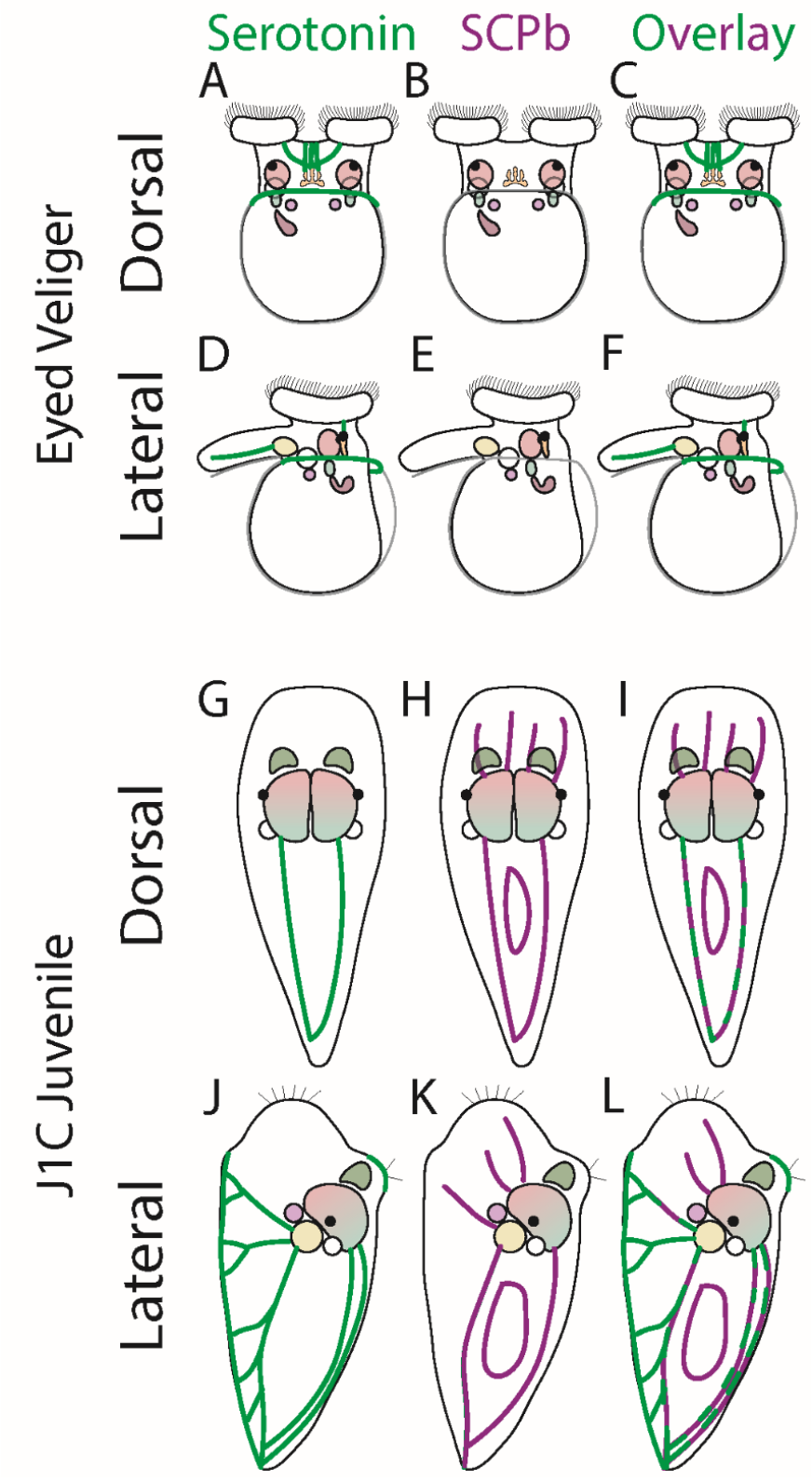
Serotonin
SCPb
Overlay
Eyed Veliger
Dorsal
Lateral
J1C Juvenile
Dorsal
Lateral
A
B
C
D
E
F
G
H
I
J
K
L

Discussion

Elongated cilia appear to mark the forming sensory organs.

Using both confocal and scanning electron microscopy, the long cilia were found at the forming sensory organs at the J1B, J1C, and later juvenile stages. The cilia were not found after right metamorphosis at the J1A juvenile, despite the noticeable formation of the rhinophore buds, and were first seen at the J1B juvenile stage. However, at the J1B stage the cilia were loosely bound and were finally tightly bound together at the J1C stage. While these cilia are significantly longer than surrounding cilia tufts, these two structures are very morphologically and functionally similar. The cilia tufts are also clustered cilia with documented PNS innervation in other species (Gobbeler, 2007) (Marois & Carew, 1997) (Chia & Koss, 1984) (Kempf & Page, 2005) (Carrigan, 2015). Thus, it is plausible that the elongated cilia may be developmental related to these cilia tufts due to their sensory function on the tips of key sensory organs. Additionally, the presence of the elongated cilia at the J1B juvenile instead of the J1A juvenile suggest there may be PNS differences between the J1A and J1B juveniles. Elongated cilia have been pictured in images of another publication using SEM to image a juvenile nudibranch (Hadfield & Pennington, 1990), but this paper did not describe this ciliated structure or identify it in their figures.

SCPb-*lir* and serotonin-*lir* in the PNS expand after metamorphosis

Metamorphosis appears to result in drastic rearrangements of the PNS in *B. stephanieae*. The PNS elements from the apical organ were identified in a previous study of *Berghia* (Carroll & Kempf, 1997), which hypothesized that those neurons played a sensory role and connected with the highly ciliated velum. Given the lack of any other notable PNS elements identified in this thesis that could serve to either innervate the velum or serve a sensory function, that hypothesis is supported by these observations. The serotonin-*lir* of the mantle edge tissue is questionable due to the intensity of the staining. This staining pattern has not been documented in other *Berghia* studies (Carroll & Kempf, 1997) (Kristof & Klussman-Kolb, 2010). While there is a possibility of trapping or other imaging artifacts, the staining is consistently seen with only serotonin-*lir* despite different laser wavelengths, secondary antibodies, and various other tested neurotransmitters. Given the isolated signaling of only serotonin, the binding of the primary antibody against serotonin appears to be real. Additionally, the loss of this activity after the mantle edge tissue is documented to retract by Carroll & Kempf, 1997 suggests it is indeed staining neurons within this tissue.

After metamorphosis, the PNS immunoreactivity expanded significantly. The diversification of innervation targets and locations could reflect the changing behavior of the post-metamorphic juvenile. Given the formation of the adult CNS at the J1C juvenile, I hypothesize that the PNS nerves identified at the J1C stage will also be found in the adult *Berghia.* Finally, while a consensus of PNS

immunoreactivity was proposed for the samples analyzed, there was a subset of immunoreactive projections that were either inconsistently found in animals, or found in a minority of animals. For example, in 2 animals analyzed, SCPb-*lir* projections from the cerebral ganglia anteriorly, ending in an immunoreactive cell. This was not seen in any other animals analyzed at the eyed veliger stage. While the cause of this inconsistency is unknown, it is hypothesized that these may be due to slight variations in age or due to modulatory nerves in the periphery which may have begun producing SCPb-*like* neurotransmitters in response to a stimulus.

PNS immunoreactivity at the J1C juvenile innervates the foot

The foot immunoreactivity found at the J1C juvenile stage is more densely packed than any other PNS element at this stage. While the purpose of this density of innervation is unknown, I hypothesize that this dense innervation prepares the animal for elongation. While the mechanisms of elongation are unknown, the rapid elongation that occurs following the J1C juvenile stage until adulthood may out-stretch the PNS. The PNS may not be equipped to replicate and differentiate the number of mature neurons needed to keep up with the elongating animal. While this hypothesis was not confirmed in this paper, supporting evidence was found.

First, the intensity of innervation in the foot may be so dense because it is preparing to be expanded. As the animal elongates, this web of neurons may stretch apart to an evenly spaced level. This would result in the foot being entirely innervated without overwhelming the ability of the PNS to rapidly generate the necessary neurons in order to maintain the innervation density seen at this stage. In order to test this hypothesis, analysis of the PNS through immunohistochemistry could be extended further into development to compare the density of foot innervation. Finally, the number of posteriorly projecting nerves and their branching nature suggests that they are prepared to elongate with the animal and serve as nerves that will innervate distinctly separate sections of the foot. This method would allow for the neuronal innervation to be established prior to the elongation of the foot. This hypothesis would prove difficult to assess, as the

identity of the ventrally branching neurons would need to be confirmed. In order to do so, lineage tracing could be used to mark a subset of PNS neurons. When combined with immunoreactivity and neural connections, identity may be able to be assumed. Then, extending later in development can measure the location along the anterior-posterior axis and the connections of these nerves as the animal elongates.

The J1C Juvenile SCP-*lir* PNS is similar to the adult *Melibe leonina*

The SCPb-*lir* PNS patterns identified in the J1C juvenile are similar to the patterns observed in the adult *Melibe leonina* (Watson, 2020) (Hurst, 1968). In the adult *Melibe*, there are 12 documented laterally paired nerves containing SCPb-*like* reactive axons. Of these 12 nerves, 5 potentially homologous nerves appeared in the J1C juvenile of *Berghia stephanieae*. First, both animals had paired nerve projections from the anterior cerebropleural ganglia into the buccal mass. Two more paired nerves run from the cerebropleural ganglia anteriorly to the mouth, or the hood in *Melibe*. The remaining hypothesized homologous neurons were the anteriorly and posteriorly running nerves from the pedal ganglia to the foot. There were 2 additional paired nerves seen in the adult *Melibe* that were not seen in *Berghia.*

Both animals contained nerves originating from the buccal ganglia that innervated the esophagus. Given the apparent homologous SCPb-*like* PNS arrangement, it is likely that these SCPb-*lir* nerves in *Berghia* will maintain the same role seen in *Melibe.* Watson, 2020 discovered that SCPb-*lir* innervation in the esophagus was sufficient to induce a contraction of the esophagus when stimulated. Additionally, when the neuropeptide SCPb was injected into *Melibe*, the animal crawled a significantly longer distance than a control injection suggesting that SCPb plays a role in locomotion. Given the similarity of PNS innervation between the two species, SCPb is hypothesized to play a similar excitatory role in *Berghia* locomotion.

Conclusions

This study provided the first description of the entire peripheral nervous system of the larval and juvenile stages of *B. stephanieae*. It was found that the PNS expanded after metamorphosis to innervate the foot, the esophagus, the gut, and the epidermis of the rhinophore. Additionally, elongated cilia were identified on the anterior surfaces of forming sensory organs. While these cilia have been documented in a previous publication (Pennington, 1990), there have been no descriptions or names of this structure in the literature. Thus, this study also provides the description of a novel sensory structure that appears to mark forming sensory organs.

Future Directions

Similarly to the CNS study in this thesis, in order to completely understand the development of the PNS throughout metamorphosis, more granularity is needed. The same development stages created in this thesis can be used to analyze the PNS and determine when immunoreactive PNS nerves arise during development. Given the inherent similarities to adult nudibranchs, a comparison of the adult *Berghia* projections from the CNS would be very useful to determine which nerves are homologous to those identified in *Melibe* and other adults. This would assist in elucidating the function of the nerves in the juvenile *Berghia*, as the function is well known in adults of other species. Secondly, the innervation of the elongated cilia at surfaces of sensory organs was not documented with SCP-*lir* or serotonin-*lir* despite the presence of epidermal innervation in these areas. In order to confirm the sensory role of these cilia and to determine where the innervation of the cilia terminates, a profile of antibodies against various neurotransmitters should be tested at the J1C or J1B stages to identify what the potential innervating neurons are immunoreactive against. Then, this innervation can be tracked developmentally to determine if the cilia or the supporting innervation arises first.

Another interesting study will be to analyze the mantle edge tissue immunoreactivity. Carroll & Kempf, 1990 documented that this mantle edge tissue retracts around the timing of the next developmental stage, the propodium veliger. Studying what happens to this immunoreactivity when this tissue retracts should be incredibly interesting. Finally, experimental confirmation of the role of SCPb

and serotonin in the juvenile and larval stages of *Berghia stephanieae* would prove very interesting given the different innervation patterns. While injections on these small animals may not be feasible, perhaps incubation in a bath with a set concentration of these neurotransmitters could produce results. This would remove the reliance upon homologous immunoreactivity patterns and then provide additional support to confirm the homology of the nerves in question.

Chapter 2, in part, is also currently being prepared for submission for publication of the material. Whitesel, CA; Johnston, HT; Lyons, DC. The thesis author was the primary investigator and author of this material.

References

Alessandri, K., Andrique, L., Feyeux, M., Bikfalvi, A., Nassoy, P., & Recher, G. (2017). All-in-one 3D printed microscopy chamber for multidimensional imaging, the UniverSlide. *Scientific Reports*, *7*(1), 42378. https://doi.org/10.1038/srep42378

Aoyagi, Y., Kawakami, R., Osanai, H., Hibi, T., & Nemoto, T. (2015). A Rapid Optical Clearing Protocol Using 2,2′-Thiodiethanol for Microscopic Observation of Fixed Mouse Brain. *PLOS ONE*, *10*(1), e0116280. https://doi.org/10.1371/journal.pone.0116280

Araújo, S. J., & Tear, G. (2003). Axon guidance mechanisms and molecules: Lessons from invertebrates. *Nature Reviews Neuroscience*, *4*(11), 910–922. https://doi.org/10.1038/nrn1243

Bonar, D. B., & Hadfield, M. G. (1974). Metamorphosis of the marine gastropod Phestilla Sibogae Bergh (nudibranchia: *Aeolidacea*). I. Light and electron microscopic analysis of larval and metamorphic stages. *Journal of Experimental Marine Biology and Ecology*, *16*(3), 227–255. https://doi.org/10.1016/0022-0981(74)90027-6

Bulloch, A. G. M., & Ridgway, R. L. (1995). Comparative aspects of gastropod neurobiology. In O. Breidbach & W. Kutsch (Eds.), *The Nervous Systems of Invertebrates: An Evolutionary and Comparative Approach: With a Coda written by T.H. Bullock* (pp. 89–113). Birkhäuser. https://doi.org/10.1007/978-3-0348-9219-3_6

Carrigan, I. D., Croll, R. P., & Wyeth, R. C. (2015). Morphology, innervation, and peripheral sensory cells of the siphon of *Aplysia californica*. *Journal of Comparative Neurology*, *523*(16), 2409–2425. https://doi.org/10.1002/cne.23795

Chia, F.-S., & Koss, R. (1984). Fine structure of the cephalic sensory organ in the larva of the nudibranch Rostanga pulchra (Mollusca, Opisthobranchia, Nudibranchia). *Zoomorphology*, *104*(3), 131–139. https://doi.org/10.1007/BF00312131

Croll, R. P., Boudko, D. Y., Pires, A., & Hadfield, M. G. (2003). Transmitter contents of cells and fibers in the cephalic sensory organs of the gastropod mollusc *Phestilla sibogae*. *Cell and Tissue Research*, *314*(3), 437–448. https://doi.org/10.1007/s00441-003-0778-1

Croll, R. P., & Voronezhskaya, E. E. (1996). Early Elements in Gastropod Neurogenesis. *Developmental Biology*, *173*(1), 344–347. https://doi.org/10.1006/dbio.1996.0028

Ellis, I. (2010). *Investigations of Neural Ontogeny in the Larval Oyster Crassostrea virginica and the nudibranch Berghia verrucicornis: A Histological and Immunohistochemical Approach* [Thesis]. https://etd.auburn.edu//handle/10415/2189

Geren, B. B., & Schmitt, F. O. (1954). THE STRUCTURE OF THE SCHWANN CELL AND ITS RELATION TO THE AXON IN CERTAIN INVERTEBRATE NERVE FIBERS*. *Proceedings of the National Academy of Sciences of the United States of America*, *40*(9), 863–870.

Göbbeler, K., & Klussmann-Kolb, A. (2006). Paddle cilia on the cephalic sensory organs (CSOs) of Opisthobranchia (Mollusca: Gastropoda) – genuine structures or artefacts? *Bonner Zoologische Beiträge*, 8.

Hegedűs, E., Kaslin, J., Hiripi, L., Kiss, T., Panula, P., & Elekes, K. (2004). Histaminergic neurons in the central and peripheral nervous system of gastropods (*Helix*, *Lymnaea*): An immunocytochemical, biochemical, and electrophysiological approach. *Journal of Comparative Neurology*, *475*(3), 391–405. https://doi.org/10.1002/cne.20171

Hurst, A. (1968). The feeding mechanism and behaviour of the opisthobranch *Melibe leonina*. *Undefined*. /paper/The-feeding-mechanism-and-behaviour-of-the-Melibe-Hurst/b9e1e8a359ac9da1db7dbaffcb989125c98997e6

Katz, P. S., & Quinlan, P. D. (2019). The importance of identified neurons in gastropod molluscs to neuroscience. *Current Opinion in Neurobiology*, *56*, 1–7. https://doi.org/10.1016/j.conb.2018.10.009

Kempf, S. C., & Page, L. R. (2005). Anti-Tubulin Labeling Reveals Ampullary Neuron Ciliary Bundles in Opisthobranch Larvae and a New Putative Neural Structure Associated With the Apical Ganglion. *The Biological Bulletin*, *208*(3), 169–182. https://doi.org/10.2307/3593149

Levy, M., Blumberg, S., & Susswein, A. J. (1997). The rhinophores sense pheromones regulating multiple behaviors in *Aplysia fasciata*. *Neuroscience Letters*, *225*(2), 113–116. https://doi.org/10.1016/S0304-3940(97)00200-0

Lewis, S. L., Lyons, D. E., Meekins, T. L., & Newcomb, J. M. (2011). Serotonin Influences Locomotion in the Nudibranch Mollusc *Melibe leonina*. *The Biological Bulletin*, *220*(3), 155–160. https://doi.org/10.1086/BBLv220n3p155

Lloyd, P. E., Frankfurt, M., Stevens, P., Kupfermann, I., & Weiss, K. R. (1987). Biochemical and immunocytological localization of the neuropeptides FMRFamide, SCPA, SCPB, to neurons involved in the regulation of feeding in *Aplysia*. *Journal of Neuroscience*, *7*(4), 1123–1132. https://doi.org/10.1523/JNEUROSCI.07-04-01123.1987

Marois, R., & Carew, T. J. (1997). Fine Structure of the Apical Ganglion and Its Serotonergic Cells in the Larva of *Aplysia californica*. *The Biological Bulletin*, *192*(3), 388–398. https://doi.org/10.2307/1542748

Marois, Rene, & Carew, T. J. (1990). The gastropod nervous system in metamorphosis. *Journal of Neurobiology*, *21*(7), 1053–1071. https://doi.org/10.1002/neu.480210710

Matsuo, R. (2017). The Computation and Robustness of the Mini-Cognitive Centers of Terrestrial Mollusks: An Exquisite Outcome of Brain Evolution. In S. Shigeno, Y. Murakami, & T. Nomura (Eds.), *Brain Evolution by Design* (pp. 101–122). Springer Japan. https://doi.org/10.1007/978-4-431-56469-0_5

McClellan, A. D., Brown, G. D., & Getting, P. A. (1994). Modulation of swimming in *Tritonia*: Excitatory and inhibitory effects of serotonin. *Journal of Comparative Physiology A*, *174*(2). https://doi.org/10.1007/BF00193792

Miller, J. A., & Byrne, M. (2000). Ceratal autotomy and regeneration in the aeolid nudibranch *Phidiana crassicornis* and the role of predators. *Invertebrate Biology*, *119*(2), 167–176. https://doi.org/10.1111/j.1744-7410.2000.tb00005.x

Minichev, Y. S. (n.d.). *ON THE ORIGIN AND SYSTEM OF NUDIBRANCHIATE MOLLUSCS (GASTROPODA OPISTHOBRANCHIA)*. 15.

Newcomb, J. M., Fickbohm, D. J., & Katz, P. S. (2006). Comparative mapping of serotonin-immunoreactive neurons in the central nervous systems of nudibranch molluscs. *Journal of Comparative Neurology*, *499*(3), 485–505. https://doi.org/10.1002/cne.21111

Newcomb, J. M., & Katz, P. S. (2007). Homologues of serotonergic central pattern generator neurons in related nudibranch molluscs with divergent behaviors. *Journal of Comparative Physiology A*, *193*(4), 425–443. https://doi.org/10.1007/s00359-006-0196-4

Nezlin, L. P., & Voronezhskaya, E. E. (2017). Early peripheral sensory neurons in the development of trochozoan animals. *Russian Journal of Developmental Biology*, *48*(2), 130–143. https://doi.org/10.1134/S1062360417020060

Pennington, T. (1990). NATURE OF THE METAMORPHIC SIGNAL AND ITS INTERNAL TRANSDUCTION IN LARVAE OF THE NUDIBRANCH PHESTILLA SIBOGAE. *BULLETIN OF MARINE SCIENCE*, *46*, 10.

Sakurai, A., Newcomb, J. M., Lillvis, J. L., & Katz, P. S. (2011). Different Roles for Homologous Interneurons in Species Exhibiting Similar Rhythmic Behaviors. *Current Biology*, *21*(12), 1036–1043. https://doi.org/10.1016/j.cub.2011.04.040

Shigeno, S., Murakami, Y., & Nomura, T. (Eds.). (2017). *Brain Evolution by Design: From Neural Origin to Cognitive Architecture*. Springer Japan. https://doi.org/10.1007/978-4-431-56469-0

VALDÉS, Á. (2004). Phylogeography and phyloecology of dorid nudibranchs (Mollusca, Gastropoda). *Biological Journal of the Linnean Society*, *83*(4), 551–559. https://doi.org/10.1111/j.1095-8312.2004.00413.x

Voronezhskaya, E. E., & Elekes, K. (2003). Expression of FMRFamide gene encoded peptides by identified neurons in embryos and juveniles of the pulmonate snail *Lymnaea stagnalis*. *Cell and Tissue Research*, *314*(2), 297–313. https://doi.org/10.1007/s00441-003-0800-7

Voronezhskaya, E. E., & Ivashkin, E. G. (2010). Pioneer neurons: A basis or limiting factor of lophotrochozoa nervous system diversity? *Russian Journal of Developmental Biology*, *41*(6), 337–346. https://doi.org/10.1134/S1062360410060019

Watson, W H, III, Nash, A., Lee, C., Patz, M. D., & Newcomb, J. M. (2020). The Distribution and Possible Roles of Small Cardioactive Peptide in the Nudibranch *Melibe leonina*. *Integrative Organismal Biology*, *2*(obaa016). https://doi.org/10.1093/iob/obaa016

Watson, Winsor H., Newcomb, J. M., & Thompson, S. (2002). Neural Correlates of Swimming Behavior in *Melibe leonina*. *The Biological Bulletin*, *203*(2), 152–160. https://doi.org/10.2307/1543384

Watson, Winsor H., & Willows, A. O. D. (1992). Evidence for homologous peptidergic neurons in the buccal ganglia of diverse nudibranch mollusks. *Journal of Neurobiology*, *23*(2), 173–186. https://doi.org/10.1002/neu.480230208

Wertz, A., Rössler, W., Obermayer, M., & Bickmeyer, U. (2006). Functional neuroanatomy of the rhinophore of *Aplysia punctata*. *Frontiers in Zoology*, *3*(1), 6. https://doi.org/10.1186/1742-9994-3-6

Whitington, P. M. (1993). Axon guidance factors in invertebrate development. *Pharmacology & Therapeutics*, *58*(3), 263–299. https://doi.org/10.1016/0163-7258(93)90025-9

Wiens, B. L., & Brownell, P. H. (1995). Neurotransmitter regulation of the heart in the nudibranch *Archidoris montereyensis*. *Journal of Neurophysiology*, *74*(4), 1639–1651. https://doi.org/10.1152/jn.1995.74.4.1639

Wyeth, R. C., & Willows, A. O. D. (2006). Odours detected by rhinophores mediate orientation to flow in the nudibranch mollusc, *Tritonia diomedea*. *Journal of Experimental Biology*, *209*(8), 1441–1453. https://doi.org/10.1242/jeb.02164

Yurchenko, O. V., Skiteva, O. I., Voronezhskaya, E. E., & Dyachuk, V. A. (2018). Nervous system development in the Pacific oyster, *Crassostrea gigas* (Mollusca: Bivalvia). *Frontiers in Zoology*, *15*(1), 10. https://doi.org/10.1186/s12983-018-0259-8